Real-time Structural Stability of Domes through Limit Analysis: Application to St. Peter's Dome

Article *in* International Journal of Architectural Heritage · October 2021

DOI: 10.1080/15583058.2021.1992539

4 authors:

Marco Francesco Funari
University of Minho
40 PUBLICATIONS **464** CITATIONS
SEE PROFILE

Luís Carlos Silva
Politecnico di Milano
34 PUBLICATIONS **252** CITATIONS
SEE PROFILE

Elham Mousavian
University of Naples Federico II
28 PUBLICATIONS **99** CITATIONS
SEE PROFILE

Paulo B. Lourenco
University of Minho
1,126 PUBLICATIONS **21,189** CITATIONS
SEE PROFILE

This paper can be found at: http://dx.doi.org/10.1080/15583058.2021.1992539

Real-time structural stability of domes through limit analysis: application to St. Peter's dome

Marco Francesco Funari[a]*, Luis Carlos Silva[b], Elham Mousavian[c], Paulo B. Lourenço[a]

[a]*Department of Civil Engineering, University of Minho, ISISE, Guimarães, Portugal*

[b]*Department of Civil Engineering, Lusófona University, ISISE, Lisbon, Portugal*

[c] *Department of Structures for Engineering and Architecture, Department of Civil Engineering, University of Naples Federico II, Naples, Italy*

Provide full correspondence details here including e-mail for the *corresponding author

Marco Francesco Funari
Postdoctoral Researcher in Structural Engineering
ISISE, Institute of Science and Innovation for Bio-Sustainability (IB-S)
University of Minho, Guimarães, Portugal
e-mail: marcofrancesco.funari @civil.uminho.pt

This paper can be found at: http://dx.doi.org/10.1080/15583058.2021.1992539

Real-time structural stability of domes through limit analysis: application to St. Peter's dome

A digital tool is presented and made available for the rapid structural assessment of historic masonry domes. It is especially suited for masonry domes that present long meridian cracks; ergo partitioned slices governed by a pushing failure mode. The proposed procedure considers a Heyman's no-tension mechanical model that has been implemented within a user-friendly visual programming environment. The numerical approach includes parametric modelling of the failure mechanism that allows exploring the domain of solutions using the kinematic theorem of limit analysis. A heuristic search method is subsequently adopted to refine the geometry of the collapse mechanism and to compute the value of the horizontal trust. Validation of the results has been achieved considering St. Peter's dome. As reported in the literature, the behaviour of this dome shifted from a rigid shell-type – stiffened by hoop stresses – towards a pushing type of dome partitioned by long meridian cracks. Unlike time-consuming and advanced methods of analysis, the present procedure allows the users to perform a structural assessment of a historic masonry dome in few seconds and offers the possibility of including: (i) the dome's drum in the analysis, if applicable; and (ii) rings as strengthening measure, whose number, position (dome or drum) and material (capacity) are user-defined. The goal is to make the tool easily and freely at the disposal of students, researchers, and structural engineers.

Keywords: St Peter's dome; historic masonry domes; kinematic limit analysis; easy to use tool for limit analysis

1. Introduction

Ancient masonry domes are widely spread across the world. The majority were designed based on rules of thumb (Gaetani, et al. 2016; Huerta Fernandez 1990; Brumana, et al. 2018; Di Croce, Ponzo, and Dolce 2010) and recent earthquakes raised the awareness over its significant vulnerability to horizontal loads (Silva, et al. 2018; Sorrentino, et al. 2013). Remedial actions based on structural assessment studies using scientific-based approaches shall be conducted (Fanning, and Boothby 2001). Still, the

structural assessment of ancient masonry domes remains a challenge. The complexity arises from the geometric arrangement of the masonry (G. Milani, and Cecchi 2013), from the phenomenological complexity of masonry mechanical behaviour (P.B. Lourenço 1997), from the uncertainty when modelling the dome's potential load paths, from the damage-induced anisotropy, and from lack of data in engineering applications. Studies that somehow allow lessening the preceding difficulties are then of prime importance, such as studies that address ancient construction methods (Gaetani, et al. 2016), advances on non-destructive testing methods (López López, et al. 2019), advances on strengthening techniques, and advances on numerical strategies of structural analysis. In this scope, the present study provides a contribution to the structural analysis of masonry domes. In fact, researchers have, in the last decades, overtly sought the improvement of structural analysis tools and different strategies have enriched the literature (Como 2019; Cennamo, and Cusano 2020; Anselmi, Galizia, and Saetta 2020; Ginovart, Costa, and Fortuny 2013; Fabbrocino, et al. 2020) since the modern theory of limit analysis proposed by Heymann (Heyman 1966; 1969). Analytical or semi-analytical approaches based on limit analysis theorems can be found (Como 2019; Pepe, Pingaro, and Trovalusci 2021; Pepe, et al. 2020; Portioli, et al. 2014; Chiozzi, et al. 2017; G. Milani, Lourenço, and Tralli 2006), but more attention has been given to numerical strategies based on the Finite Element (FE) (Fortunato, Funari, and Lonetti 2017) and Discrete Element (DE) (Mehrotra, Arede, and DeJong 2015; Savalle, Vincens, and Hans 2020; Simon, and Bagi 2014) methods.

FE-based strategies have perhaps received more attention because most commercial software codes adopt the FE method. FE models allow the modelling of masonry either through a continuous and homogeneous representation of the media (macro-modelling) (Cascardi, et al. 2020; Silva, et al. 2018) or through an explicit

discretization of both units and joints (micro-modelling) (Lemos 2007). Mechanical behaviour of the masonry is typically achieved through non-linear constitutive laws. Due to the high computational effort required, micro-modelling is still devoted for small-scale studies and within a non-linear static analysis. In converse, the appropriateness of a macro-modelling is well recognizable for the study of larger scale structures and within both non-linear static and dynamic types of analysis. For instance, Bacigalupo et al. (Bacigalupo, Brencich, and Gambarotta 2013) developed a macroscopic FE model and performed non-linear quasi-static analyses for the structural assessment of S. Maria Assunta's dome and drum in Carignano; and Cavagli and Gusella (Cavalagli, and Gusella 2014) studied the dome of the Basilica of Santa Maria degli Angeli in Assisi through a non-linear quasi-static analysis. Bartoli et al. (Bartoli, Betti, and Borri 2015) also developed a macroscopic FE model to perform the structural analysis of Brunelleschi's Dome of Santa Maria del Fiore, in which both static and dynamic types of analysis were considered. Hejazi and Pourabedin (Hejazi, and Pourabedin 2021) analysed several domes under seismic loads by means FE non-linear models. A Willam-Warnke failure criterion was adopted to identify the crushing of brick masonry. Recently, Feizolahbeigi et al. (Feizolahbeigi, et al. 2021) developed a numerical study to analyse the influence of geometry and construction techniques on the seismic behaviour of bulbous discontinuous double shell domes in central Iran. An advanced FE model limited to the dome-drum system was considered. Diz-Mellando et al. (Diz-Mellado, et al. 2021) performed a multidisciplinary study about the Seville Cathedral. Data from non-destructive tests allowed the calibration of the FE model. The authors stated that the leading cause of damage was caused by the dome's horizontal thrusts on the lateral façades.

Advances on the available FE analysis tools have not eased, by itself, the structural assessment of masonry domes. These require a significant amount of data and can be both time-consuming and computationally expensive, especially when trying to model collapse and estimate the ultimate ductility level of the dome (Gabriele Milani, Simoni, and Tralli 2014). Powerful analytical tools based on the theorem of the limit analysis can be an appropriate alternative (Turco, et al. 2020; M.F. Funari, et al. 2020; Heyman 1966). Limit analysis approaches require fewer mechanical parameters input and are, therefore, more practical. Several authors developed advanced tools based on the lower and upper bound theorems of limit analysis. Cennamo et al. (Cennamo, and Cusano 2020) investigated the shape and seismic vulnerability of San Francesco of Paola's dome in Naples, whereas a lower bound theorem of limit analysis was used through a graphical approach. Similarly, Anselmi et al. (Anselmi, Galizia, and Saetta 2020) proposed a computer program based on the static theorem of the limit analysis that demands only an a priori discretization of the dome in macroblocks. The Upper Bound theorem of limit analysis is extensively adopted to assess arches and domes' horizontal thrust. In this case, the computation of the load multiplier depends on the geometry of macroblocks. Multiple (theoretically infinite) failure mechanisms hence need to be considered to evaluate the minimum of the kinematically compatible load multipliers (Maria D'altri, et al. 2020). For this purpose, researchers have been adopting useful optimization routines that solve the minimization problem constrained under specific hypotheses (Marco Francesco Funari, Mehrotra, and Lourenço 2021). For instance, Milani (G. Milani 2015) proposed a numerical procedure based on a discontinuous upper bound limit analysis approach with sequential linear programming mesh adaptation to analyse masonry vaults. Furthermore, the development of limit analysis tools that are easily adapted to perform ad-hoc studies is quite convenient,

especially since historic domes have intrinsic particularities. In this regard, researchers are addressing the importance of graphical interfaces and automatic procedures, as they may foster the use of these tools within engineering practice. For instance, Funari et al. (Marco Francesco Funari, et al. 2020; M.F. Funari, et al. 2020) proposed the modelling of a parametrized macro-block that, through advanced optimization and visual scripts, allowed for exploring the domain of possible solutions using the upper bound method of limit analysis. Block et al. (Block, Ciblac, and Ochsendorf 2006; Rippmann, Lachauer, and Block 2012) have also developed interactive tools based on three-dimensional thrust network analysis and implemented it in the Rhino 3D software. A strategy based on the static theorem of limit analysis, with background on the O'Dwyer works (O'Dwyer 1999), was proposed and able to describe the equilibrium of compressive funicular networks.

In such context, the present paper fundamentally aims to develop a numerical tool for the structural assessment of masonry domes through a limit analysis formulation. It is intended to be: (i) freely available for the use of students, scholars, and practitioners; (ii) computationally fast and efficient; (iii) implemented within a visual script (Rhino 3D) platform and easy to use; and (iv) able to provide real-time results with the geometry update. The worldwide known St. Peter's dome in Rome has been selected as a benchmark. A FE numerical model via a macro-modelling approach serves as a reference for the comparison of the horizontal thrust capacity. Because of its significance, as well as its damaged state, St. Peter's dome has been extensively studied in the past by academics (Poleni 1982; Le Seur, Jacquier, and Boscovich 1742), structural engineers ("The Dome of St Peter's: Structural Aspects of Its Design and Construction, and Inquiries into Its Stability on JSTOR" 1999; Como 2019), and architects (Baldrati 2009). Recently, Como (Como 2019) studied the history of the

structural assessment of the St. Peter's dome and introduced some developments of the limit analysis applied to masonry providing an evaluation of the horizontal thrust by using the upper bound theorem of the limit analysis, which is adopted here. Baldrati (Baldrati 2009) published the result of a detailed work based on the usage of non-destructive testing for the characterization of construction techniques and processes adopted in the site. De Sanctis et al. (De Sanctis, et al. 2018) analysed the structural surveys performed between the 17th and the 18th centuries and developed a detailed three-dimensional model of St. Peter's dome. Several works exist, but an advanced numerical simulation aimed at the structural assessment of the St. Peter's dome is still lacking. Recent work by Jasieńko et al. tried to cope with the latter (Jasieńko, et al. 2021), in which an elasto-plastic three-dimensional numerical model of the dome and drum was developed. However, only the non-strengthened configuration was considered, which does not represent the current state (strengthened with six iron rings) of the dome.

In this regard, the paper addresses the implementation of an upper bound limit analysis tool that will be freely available. Its validation will be achieved using the St. Peter's dome as a benchmark and the results provided, given in terms of the dome's horizontal thrust, will be put against those obtained with a macroscopic FE model. Both non-strengthened and strengthened (iron rings) configurations of St. Peter's dome will be considered. Important remarks are also addressed for a rational computation on the tension force of iron rings within the FE model, which seems to be a contentious issue in the literature. The paper is organized as follows: section 2 includes the framework adopted and the objectives; section 3 describes, in brief, the history of the case study; section 4 includes the description of the FE numerical modelling for both the non-strengthened and strengthened configurations of St. Peter's dome; section 5 addresses

the implementation of the kinematic limit analysis tool; section 6 reports the discussion of the results found, in terms of horizontal thrust and damage pattern, between the kinematic limit analysis and FE model; section 7 provides an overview on the static efficiency of St. Peter's dome and a comparison with other well-known ancient domes; and finally, section 8 reports the main conclusions.

2. Framework and Objectives

The primary goal of the study is the implementation and validation of a structural analysis tool for masonry domes. The tool is based on the limit analysis and within an upper-bound (kinematic) formulation given by Como (Como 2019). To accomplish the latter, the framework described next has been followed:

(1) Modelling the geometry of St. Peter's dome, which may be subsequently used for the structural analysis. The modelling of the dome may be developed in the software Rhino 3D + Grasshopper ("Rhino - Rhinoceros 3D" 2020; "Grasshopper - Algorithmic Modeling for Rhino" 2020) to fully take advantage of the automatic procedure concerning the limit analysis tool. See Section 3.

(2) Development of an advanced FE numerical model to serve as a reference for the validation of the limit analysis tool. A three-dimensional numerical model based on the Finite Element (FE) method and following a macro-modelling approach was assumed. Such choice is supported by an extensive literature that used FE model to numerical assess masonry structures in general, and domes in particular (Gabriele Milani, et al. 2019; Scacco, Milani, and Lourenço 2020; Jasieńko, et al. 2021; Fanning, and Boothby 2001; Bacigalupo, Brencich, and Gambarotta 2013; Bartoli, Betti, and Borri 2015; Cavalagli, and Gusella 2014). See Section 4.

This paper can be found at: http://dx.doi.org/10.1080/15583058.2021.1992539

(3) Implementation of the kinematic limit analysis strategy within a Rhino 3D + Grasshopper ("Rhino - Rhinoceros 3D" 2020; "Grasshopper - Algorithmic Modeling for Rhino" 2020) plugin. Such a plugin includes Grasshopper (GH) components to analyse the non-strengthened and strengthened dome configurations. By strengthening, it is meant the retrofit through iron rings, but ultimately the tool may be able to represent other materials. The plugin will be developed using Python programming language. As output, the tool may provide the dome's horizontal thrust and the position of the failure mechanism (position of the rotational hinge of the failure mechanism). See Section 5.

(4) Comparison of the results obtained by the kinematic limit analysis and the FE numerical model. Maximum horizontal thrust will be compared, together with the expected failure mechanism for the studied non-strengthened and strengthened configurations. See Section 6.

The novelties of the study are twofold and are addressed next:

- Develop a limit analysis tool based on the upper bound theorem that is fast and easy to use. The tool may allow the computation of the thrust force and expected failure mechanism for a given dome in few seconds. Additionally, it will be made available online as a shareable Grasshopper ("Grasshopper - Algorithmic Modeling for Rhino" 2020) component.
- Application of the developed kinematic limit analysis tool and a numerical FE model or the assessment of the structural behaviour and static efficiency of St. Peter's dome, one of the most well-known and iconic domes of the world.

The intrinsic features required to perform the structural assessment of St. Peter's dome also constitute, by itself, key points and are recognized to be valuable contributions. For

instance:

- The kinematic tool can be used within a sequential type of analysis. The structural assessment of domes typically requires the assessment at different stages to follow its historic evolution and related modifications. Herein, three stages are especially addressed, whose differences are given in terms of the number and position of iron rings. The tool includes the structural effect of the iron rings by prescribing the tension force of these members as input parameters.
- Modelling the contribution of the iron rings in a FE model within a rational basis. The computation of the tension force provided by the confinement effect of the latter rings is based on a mechanistic formulation and is addressed in section 4.3.

3. St. Peter's Dome

3.1. Historical overview

The Papal Basilica of St. Peter, also known as St. Peter's Basilica and given in Figure 1a, is located in the Vatican City, which is by itself a UNESCO world heritage cultural site ("Vatican City - UNESCO World Heritage Centre" 2021). The Basilica is a prime example of Renaissance style and one of the most famous and important monumental sites of the world, as it gathers invaluable historical, religious, and cultural values. St. Peter's dome is presented in Figure 1b and was built between 1506 and 162 , being worldwide known for its remarkable size and architectural features. The dome was selected as a case study aiming to employ and prove the capabilities of the proposed limit analysis tool.

The original concept for the Basilica's dome was idealized by Michelangelo, being then slightly modified by G. Della Porta that: (i) redefined its profile aiming to

This paper can be found at: http://dx.doi.org/10.1080/15583058.2021.1992539

achieve an alike shape with the Florence domes designed by Brunelleschi, and (ii) introduced two iron rings. The latter elements were revealed to be essential, as allowed to sustain the dome in the aftermath of the seismic events that occurred in 1703 and 1730 (Como 2019).

Some damage was reported only fifty years after its completion and Pope Innocenzo XI commissioned Carlo Fontana to perform a new structural survey. Although a favourable conclusion on the dome stability was retrieved and retrofit interventions considered to be unnecessary (Fontana 1694), the election of Pope Benedict XIV brought the opportunity to a new structural assessment conducted by L. Vanvitelli. Such study, performed in the mid-18th century, revealed that the drum and the attic were rotating outwards causing the onset of meridian cracks that lead to the split of the dome in several pushing arches. This is undesirable from a structural standpoint as these arches behave independently and the membrane effect is lost. A possible cause for such damage is the poor capacity of the foundations, as addressed in (Macchi 2001), that led to settlements.

At the same time (around 1742), three famous mathematicians (Le Seur, Jacquier, and Boscovich 1742) published two reports that included both a detailed survey of the dome and an experimental campaign to assess the mechanical properties of materials. A simple graphical-based analysis (similarly to a one-dimensional bar problem) was also developed to identify the dome's thrust. Three main conclusions were stated: (i) the base of the drum was damaged, (ii) the buttresses had a significant crack pattern, and (iii) the drum and the buttresses were undersized. The Three Mathematicians proposed a strenuous strengthening intervention, which would have modified Michelangelo and Della Porta's original architectural concept. In this regard, Pope Benedict XIV decided to follow the recommendations of another brilliant scholar,

Giovanni Poleni (Poleni 1982). In *Memorie istoriche* (Poleni 1982), Poleni assessed the previous works and presented, in a detailed way, the main outcomes. It was concluded that St. Peter's dome was adequately designed, and non-invasive interventions were proposed to keep the original architecture. During the retrofitting works, Vanvitelli realized that one of the original iron rings was broken and, possibly, a second one could be damaged too. Although initially unplanned, a total of six iron rings encircling the dome were added. Figure 2 presents the structural modifications conducted in the St. Peter's dome by Poleni.

3.2. Geometrical features

Geometrical and structural details necessary to complete a three-dimensional model were obtained from existing data collected during the surveys from the 17th and 18th centuries. Such data was also used to produce accurate drawings for the damage assessment of the dome, as given in (Poleni 1982; Le Seur, Jacquier, and Boscovich 1742). The dome has a height, from its base to the outer extrados shell, of 28.8 m and a diameter of 42.7 m. It is composed of two interconnected shells stiffened by 16 ribs. The thickness of the internal and external shells are, respectively, 2.0 m and 1.0 m, and the total thickness of the dome ranges from 3.00 m. at its base, up to 5.40 m at the crown.

More recently, Bussi et al. (Bussi, Carusi, and Rocchi 2009) performed a three-dimensional survey of the Vatican dome's intrados, through a terrestrial laser scanning procedure that validated the historical drawings. The works from Bucci et al. (Bussi, Carusi, and Rocchi 2009) lacked, however, information over the dome's extrados, as it is covered by a lead cladding that made it undetectable to trace with the later technology. In this context, the geometrical modelling of the St. Peter's dome, which includes the attic-drum-buttresses structural system, was achieved through information

gathered from the terrestrial laser scanning and Carlo Fontana's historical drawings (Fontana 1694).

St. Peter's dome features double symmetry that enables the use of a representative reduced model. The most rational choice is the study of 1/16 slice defined by the existing 16 ribs, as demonstrated in Figure 3a. Following the available literature data, the ribs were considered to have an angular span of 5 degrees (Figure 3b). Furthermore, both the intrados and extrados profiles follow the perimetral configuration of the auxiliary circles that are depicted in Figure 3b. The centres of such arches lie outside the vertical symmetry axis, which is of particular interest for the parametrization of the geometry.

4. Numerical Finite Element (FE) Model

This section includes the development of a finite element (FE) model of St. Peter's dome. The required tasks are addressed next and include the parametrization of the geometry, FE mesh discretization, the description of the mechanical behaviour for structural materials, the definition of the boundary conditions, and the application of the loading conditions.

4.1. FE mesh

St. Peter's dome symmetry enables the use of a reduced model that allows saving both computational time and resources. The 1/16 dome slice used to represent the dome's global mechanical behaviour is given in Figure 4a. Geometrical modelling and parametrization were developed using the software Rhino 3D ("Rhino - Rhinoceros 3D" 2020) since it allows to efficiently represent spatial geometries through a non-uniform rational B-splines (NURBS) approach. Attention was given to remove potential imperfections within the NURBS model, such as self-intersections and voids, as it may

affect the consistency and quality of the FE mesh. A tolerance-based criterion was used to correct such imperfections.

The FE model was prepared in the advanced commercial software ABAQUS CAE (Abaqus 2014). Although any advanced structural analysis software could be used, as it serves only for validation purposes for the limit analysis tool, ABAQUS CAE was adopted since it has been largely used for the study of quasi-brittle materials, see (Lubliner, et al. 1989).

At this stage, and following the framework described in section 2, the interoperability between the software's used for the geometric modelling (Rhino 3D) and structural analysis (ABAQUS CAE (Abaqus 2014)) is explored (via IGES file format).

Concerning the boundary conditions, symmetry has been respected by fixing the base of the slice, given by the interface with the drum/buttresses system, and by restricting the horizontal displacements to zero at the crown of the dome (Figure 4b). Furthermore, an important modelling remark is that the existing damage – given by meridian cracks – leads to the loss of the membrane effect at an ultimate limit state. These slices act as flying buttresses and hoop stresses can be disregarded; hence it is possible to study only 1/16 slice of the dome. Another modelling consequence is that restricting the lateral displacements through the dome profile becomes unnecessary.

The loading conditions are given also in Figure 4b and include two load cases: (i) the self-weight of the dome; and (ii) the weight of the lantern. Although both load cases are of permanent nature, its distinction is required considering the type of analysis performed next. A quasi-static analysis is planned, meaning that the dome's weight is firstly applied, and after the lantern's weight is incrementally applied, i.e. by following the so-called push-down analysis.

This paper can be found at: http://dx.doi.org/10.1080/15583058.2021.1992539

The three-dimensional FE model enforces the use of three-dimensional (solid) FE's and, therefore, the mesh discretization was achieved using tetrahedron (Delaunay) FE's due to its adaptability to more complex geometries. The so-called TETC3D4 finite elements in ABAQUS CAE (Abaqus 2014), based on a tetrahedral geometry with linear interpolation, were used. The final FE numerical model has a total of 149,058 tetrahedral elements and, considering interelement continuity, the number of nodes is equal to 30,526 (Figure 4c).

4.2. Mechanical behaviour for the masonry

St. Peter's dome was constructed within a lime-based mortared masonry, which was largely used in the Basilica, designated as *Fabbrica di San Pietro* (according to historic documents (Baldrati 2009)). The so-called macro-modelling approach was followed, meaning that the masonry arrangement is smeared out in a homogeneous material. This is especially convenient for the analysis of large-scale structures (Paulo B. Lourenço, and Silva 2020). ABAQUS (Abaqus 2014) offers the possibility to reproduce the macroscopic masonry mechanical behaviour through several models, e.g. the smeared crack concrete, the brittle crack concrete, and the concrete damage plasticity (CDP) models. Herein, the CDP model was used since it is suitable for quasi-brittle materials in general (Lubliner, et al. 1989). It couples plasticity with a scalar-based damage model and, as it was originally developed for concrete, an elastic isotropic behaviour is assumed. This is a limitation when adapting CDP to masonry, as orthotropy may have an important role, especially in presence of a periodic masonry arrangement (Sharma, et al. 2021; Willis, Griffith, and Lawrence 2004). The fact that masonry orthotropy is lost does not constitute a contentious issue for the present case study. It is important to note that in large-scale structures as St. Peter's dome, well-marked and fixed orthotropy directions are hard to find as a plethora of masonry arrangements may exist. The

importance of orthotropy is somehow lessened, and isotropic behaviour is an acceptable simplification. CDP can also account for different strength values, post-peak behaviours, and damage descriptions to be assigned for the tensile and compressive regimes and include a cohesive frictional behaviour for the shear regime. CDP has been extensively used for the study of large masonry structures (Cundari, Milani, and Failla 2017; Fortunato, Funari, and Lonetti 2017), and the results indicate that it offers a good compromise between computational time and accuracy.

Material response is described in terms of effective stress and strain curves, see Figure 5a. The quasi-brittle nature of masonry was represented by a linear type of softening in tension. In compression, a plateau exists after the compressive strength, being followed by a linear type of softening. Damage variables are adopted when softening is active and aim at reducing the initial (undamaged) elastic modulus through the following expressions:

$$\begin{aligned} \sigma_c &= (1 - d_c)E_0\left(\varepsilon_c - \varepsilon_c^{pl}\right) \\ \sigma_t &= (1 - d_t)E_0\left(\varepsilon_t - \varepsilon_t^{pl}\right) \end{aligned} \tag{1}$$

In which σ_i is the effective stress value; d is the damage parameter relating the effective stress with the corresponding inelastic strain; ε_i is the total strain value; and ε_i^{pl} is the inelastic (plastic) strain value. The subscript i reads as c or t, if associated with the compressive or tensile regime, respectively.

A scalar-based damage model describes the damage in tension d_t (cracking) and compression d_c (crushing). Parameters d_t and d_c are eligible to be a value between zero (no damage) and one (fully damaged) and are useful for the better understanding of damage progression in the masonry. The main purpose is provided, however, when cyclic loading is applied, as it allows describing the loss of stiffness in the unloading phase due to cracking and crushing. CDP assumes a non-associated flow rule given as a Drucker-Prager hyperbolic function and requires the definition of several physically

based parameters. The Drucker-Prager strength domain criterion was modified through a parameter $K_c = 2/3$ to approximate it with a Mohr-Coulomb criterion. The eccentricity parameter, which expresses the rate at which the plastic flow potential approaches the Drucker-Prager function for high confining pressure levels, was set to the default value of 0.1 (Lubliner, et al. 1989). A dilation angle of 10 degrees and a ratio between the bidirectional and unidirectional compressive strengths of masonry of 1.16 (default value (Lubliner, et al. 1989)) were assumed. A viscosity parameter of 0.002 was adopted and the analysis indicated it is an appropriate choice. These parameters are described in Table 1 and the reader is referred to (Cundari, Milani, and Failla 2017; Fortunato, Funari, and Lonetti 2017) for further details on the CDP model.

The absence of specific in situ test data enforce the use of local normative recommendations for the masonry mechanical properties. Hence recommendations reported in the Italian Building Code (Mordà, and Mancini 2018) and corresponding annex (e dei Trasporti 2019) were considered, in which a level of confidence inherent to the knowledge level is set to be as LC1. A LC1 level requires the use of a confidence factor equal to 1.35. A factor of 1.0 is however prescribed since the present study intends to provide a structural evaluation through different strategies, rather than providing a conservative assessment over the structural integrity of the Vatican's dome. The adopted mechanical properties are summarised in Table 2 : Geometrical and mechanical properties of the iron rings..

Post-peak responses are presented in Figure 5b for tension and compression regimes and serve as input for the CDP model. These curves were calibrated considering the damage for the non-strengthened configuration reported in the existing literature (Como 2019) in the aftermath of earthquake events of 1703 and 1730. In this regard, the tensile and compressive post-peak responses were tuned, aiming to reach the

following damage at collapse: extensive cracking at the dome's rib, diagonal cracking at the buttresses, and followed by the onset of a rotational hinge at the dome's extrados.

4.3. Numerical FE models: non-strengthened and strengthened

Historical structures may suffer recurrent structural modifications during their life span, which can be caused by adaptive reuse (Sharifi 2020), degradation of structural elements, or damage caused by extreme events such as earthquakes, floods, among other causes (Prieto, et al. 2019). A sequential type of analysis may be then required when assessing its structural behaviour. In this scope, different stages were considered for the structural analysis of the Vatican dome, and Figure 6 comprehends the three studied configurations, whose major differences include the position and number of the iron rings. In specific:

- Configuration C1 (Figure 6a): absence of iron rings, as it represents the state of the dome after the earthquake of 1703;
- Configuration C2 (Figure 6b): presence of two iron rings, as it is coincident with the original design by Della Porta in the 16th century;
- Configuration C3 (Figure 6c): presence of six iron rings, as it reproduces the dome's structural behaviour after the retrofitting interventions designed by Poleni and Vanvitelli in the 18th century. Note that the iron ring in the position defined by (a) in Figure 6c was disregarded as it coincides with the position of the supports, having thus no structural role.

The iron rings presented in the C2 and C3 configurations increased the radial stiffness of the structural system and decreased the dome's thrust. Although the structural importance of such type of retrofit is well established, most of the literature works still adopt specious strategies for the representation of its structural role within numerical

models. Some researchers neglect the confinement effect provided by the rings aiming to improve the practicability of the analysis (Bacigalupo, Brencich, and Gambarotta 2013; Cavalagli, and Gusella 2014). When considered, iron rings are typically modelled via an 'equivalent' approach, in which the elastic modulus of the masonry is locally increased (Bacigalupo, Brencich, and Gambarotta 2013). Although convenient from a practical standpoint, it may blur the representativeness of the solution since the local improvement for the masonry elastic modulus lacks objectivity.

Here, the iron rings were explicitly modelled aiming to include both its axial stiffness and the corresponding confinement effect. The former is represented by assuming appropriate cross-section and material property values and modelled via FE trusses embedded in the masonry by a segment of the circle considering an angle span equal to slice's arch angle ($\pi/8$). The latter, which is mathematically more demanding, is to consider that the confinement effect is provided by FE springs connected from the idealized centre of the dome (Figure 7).

It is worth noting that the confinement effect could be simulated through trusses elements rather than linear springs, i.e. introducing an elastoplastic material behaviour. However, it is outside the scope of this paper, and such an assumption will be considered in a future study aimed to also investigate the seismic behaviour of the St. Peter's dome.

The confinement effect is thus mimicked through spring FEs linked with the iron rings that are modelled via truss FEs embedded within the masonry. A perfect connection between the rings-masonry is assumed, being the interaction defined to follow a tie type of constraint (Figure 7a). The corresponding stiffness for the springs' FEs is conditioned by the translation equilibrium of a ring's arch, as given in Figure 7c. In this regard, the static equilibrium can be written as:

This paper can be found at: http://dx.doi.org/10.1080/15583058.2021.1992539

$$\int_{\frac{-d\theta}{2}}^{\frac{d\theta}{2}} p \cdot r \cdot h \cdot cos(\theta)\ d\theta = 2 \cdot N \cdot sin\left(\frac{d\theta}{2}\right) \quad (2)$$

In which p is the radial pressure that tends to enlarge the ring; r, h, and t are the ring's radius and the cross-section dimensions, respectively; and N is the internal axial force of the rings. Through mathematical simplification, it is possible to express the internal axial force as:

$$N = p \cdot r \cdot h \quad (3)$$

By considering that the ring's thickness is significantly smaller than its radius ($t \ll r$), then a uniform stress state along the rings thickness can be assumed (Belluzzi 1946). So, the stress of the rings reads as:

$$\sigma_{ring} = \frac{N}{t \cdot h} = E_I \cdot \varepsilon_c \quad (4)$$

In which, E_I is the iron elastic modulus and ε_c the circumferential strain, which equals to the radial one:

$$\varepsilon_c = \varepsilon_r = \frac{\Delta r}{r} \quad (5)$$

Therefore, by replacing in Equation 4 the expression given for the internal axial force of the rings and the value of the circumferential strain, it may be deduced that:

$$p = k_d \cdot \Delta r \quad (6)$$

where k_d is defined as the distributed radial stiffness per unit of area and computed as:

$$k_d = \frac{E_I \cdot t}{r^2} \quad (7)$$

This paper can be found at: http://dx.doi.org/10.1080/15583058.2021.1992539

As the angle span $d\theta$ is assumed to be $\frac{\pi}{16}$ (for the present study), then the resultant tangential stiffness value K_T (in the x-direction, see Figure 7c) can be computed as:

$$K_T = k_d \cdot \frac{\pi}{16} \cdot r \cdot h \tag{8}$$

From a numerical point of view and to ensure a uniform stress distribution of the iron rings, the stiffness value computed in Equation 8 is simulated through four radial springs. Table 2 summarises the geometrical and mechanical properties of the iron rings considered in both C1 and C2. It should be noted how the cross-section area and the rings' location have been deduced by historic reports and from the recent state-of-the-art surveys.

5. Kinematic-Based Limit Analysis Tool for Domes

Masonry domes tend to develop meridional cracks due to their low hoop tensile strength (Heyman 1966). Such cracking leads to the formation of discretized slices and a weak membrane effect. Heyman (Heyman 1966) stated that the expected failure mechanism of a hemispherical dome slice, under its self-weight, is composed of four rotational hinges. However, the expected failure mechanism for the St. Peter's ribbed dome may be alike to a semi-circular arch collapse pattern rather than a hemispherical type of dome (Como 2013). Following this observation of Como (Como 2013), the computation of the minimum thrust through limit analysis is relevant.

A formulation based on the static theorem of limit analysis allows tracing the statically admissible funicular thrust network of the load. In the incipient collapse state, the thrust line passes by the extrados of the key section and a rotational hinge is expected to appear. The point at which the thrust line intersects the dome's intrados defined the second hinge location. From a computational implementation standpoint, a

kinematic theorem of limit analysis was, however, assumed in this study. In particular, the theoretical background of the developed digital analysis tool is based on Como (Como 2013). According to Como (Como 2019), the failure mechanism that allows describing the kinematic problem is presented in Figure 8a. The principle of virtual work is, therefore, adopted and the mechanism can be kinematically described through a unique parameter, the virtual displacement $\delta\vartheta$. Multiple failure mechanisms – defined by the rotational hinge position along the dome's intrados –need to be considered to evaluate the minimum of the kinematically compatible load multipliers, for which an optimization routine is used. The equation of the virtual work for the considered failure mechanism reads as:

$$W_C \cdot \frac{\delta\vartheta}{h_t} \cdot (d_t - d_C) + W_L \cdot \frac{\delta\vartheta}{h_t} \cdot (d_t - d_L) - \sum_{i=1}^{n} R_i \cdot \frac{\delta\vartheta}{h_t} \cdot h_i - \sum_{j=1}^{m} R_j \cdot \delta\vartheta - HT^D \cdot \delta\vartheta = 0 \quad (10)$$

in which the position of the hinge (red circle in Figure 8a) is defined through the variable *t*; W_C includes the inertial forces arising from the self-weight of the dome above the position of the hinge *t*; W_L is the inertial force arising from the weight of the lantern; R_i are the forces arising from the iron rings located above the position of the hinge *t* and R_j are the forces arising from the iron rings that are below the actual hinge position *t*; and $\delta\vartheta$ is the horizontal virtual displacement that describes the collapse mechanism of the dome (Como 2013). From Equation 10, one can find the horizontal thrust of the dome only (HT^D) value:

$$HT^D = W_C \cdot \frac{(d_t - d_C)}{h_t} + W_L \cdot \frac{(d_t - d_L)}{h_t} - \sum_{i=1}^{n} R_i \cdot \frac{h_i}{h_t} - \sum_{j=1}^{m} R_j \quad (11)$$

It is noteworthy to stress again that the HT^D value depends on the geometry of the failure mechanism, which is defined by the position of the hinge parametrized in terms of the length value *m* (Figure 8). For each position *m* it is possible to compute a

This paper can be found at: http://dx.doi.org/10.1080/15583058.2021.1992539

value for HT^D through Equation 11; in which the hinge position is constrained to occur between $m_a \leq m \leq m_L$ as presented in Figure 8. The latter computations lead to a set of dome's horizontal thrust values, in which the desired one is found by solving the following constraint maximization problem:

$$\{\max\ HT^D : [m_a \leq m \leq m_L] \tag{12}$$

After the computation of the dome's horizontal thrust, it is required to demonstrate if the initial assumption given by the failure mechanism reported in Figure 8b is valid. For this purpose, one must assure that the stability of the retaining system (attic-drum-buttress) caused by an overturning type of mechanism is guaranteed. In this regard, Figure 8b represents the kinematic mechanism that produces the collapse mechanism caused by the slender retaining system of the Vatican's dome. The expressions for the stabilizing and overturning virtual works read, respectively, as:

$$\delta W_S = V \cdot \frac{\delta\vartheta}{h_a} \cdot d_V + W_B \cdot \frac{\delta\vartheta}{h_a} \cdot d_B + W_D \cdot \frac{\delta\vartheta}{h_a} \cdot d_D + \sum_{k=1}^{o} R_k \cdot \frac{\delta\vartheta}{h_a} \cdot h_k \tag{12}$$

$$\delta W_O = HT^D \cdot \delta\varphi \cdot \frac{\delta\vartheta}{h_a} \tag{13}$$

In which, R_k are the forces arising from the iron rings acting along with the retaining system. The ratio $\delta W_S/\delta W_O$ defines the safety factor of the dome with respect to the condition of incipient collapse ($\frac{\delta W_S}{\delta W_O} = 1$) (viz. unstable equilibrium position). Note that the iron rings forces that can exist due to strengthening are accounted in the formulation and eligible to be located above the hinge, in between the hinge and dome's centre position, and below the centre of the dome, as depicted in (Figure 8b). In the case that an attic-drum-buttress system exists, the horizontal thrust that is transmitted by the whole system needs to be re-evaluated. This is simply given as per Equation 14:

This paper can be found at: http://dx.doi.org/10.1080/15583058.2021.1992539

$$HT = HT^{D} - \sum_{k=1}^{o} R_k \quad (14)$$

In which HT is the horizontal thrust of the whole system, which is transmitted to the sub-structure underneath (as the altar pendentives and piers, which are not represented herein); HT^{D} is the horizontal thrust of the dome and, again, R_k are the forces arising for the potential iron rings that exist in the so-called retaining system.

The limit analysis strategy was implemented within a Rhino 3D + Grasshopper (GH) plugin, as it enables both the geometric modelling and structural analysis to be fully placed and conducted together. The plugin was developed within a GhPython ("The Python Language Reference — Python 3.9.5 Documentation" 2021) script coupled with a heuristic solver based on the Nelder-Mead method (Lagarias, et al. 1998) to solve the optimization problem. It can automatically account with: (i) any dome's slice configuration and geometry; (ii) existence of iron rings whose number and position are user-defined, of particular interest when analysing different strengthening solutions; and (iii) existence of the so-called retaining system (Figure 8b) composed by attic-drum-buttress. Therefore, the study of the non-strengthened dome (configuration C1), the strengthened dome with two iron rings (configuration C2), and the strengthened dome with six iron rings (configuration C3) can be analysed using the same tool and the associated safety factors estimated in a matter of seconds.

6. Results and Discussion: FE Model vs Kinematic Limit Analysis

Validation of the limit analysis procedure is presented next. Horizontal thrust (HT) values for C1, C2, and C3 configurations are reported and compared with those got from a non-linear FE numerical model. A reduced model is given by a 1/16 slice of the dome – as addressed in section 4– due to the revolving symmetry feature of St. Peter's dome. Before delving into the discussion of the results, it is noteworthy stressing that an

This paper can be found at: http://dx.doi.org/10.1080/15583058.2021.1992539

incremental non-linear FE analysis was performed following a push-down type of analysis. In specific, the dome's self-weight was firstly applied, being followed by the application of the lantern weight conditioned by the load multiplier λ_{WL}.

6.1. Configuration C1: horizontal thrust of the dome

C1 configuration represents the condition of the dome after the earthquake events of 1703 and 1730, in which the existing iron rings u and n (Poleni 1982) have failed. The stability of the dome without tension rings is assessed, and the obtained results are given in Figure 9. FE results provide the system horizontal thrust (HT) evolution as a function of the vertical displacement at the dome's crown (set as control point). Damage patterns are characterized by the damage parameter in tension d_t have been also plotted for different instants associated with different lantern load multipliers λ_{WL}. Results show no evidence of tension damage when the dome is subjected to its self-weight ($\lambda_{WL} = 0$). The continuous increment of the lantern weight until $\lambda_{WL} = 1.0$ leads to the increase of the horizontal thrust up to a value of 2289 kN. It is rather clear that for this load level, a rotational hinge is already active and at the dome's intrafos. A maximum force capacity of 1.02 is obtained with the non-linear FE model in which the existing previous damage is further propagated.

The strategies show an excellent agreement since the maximum horizontal thrust got via FE analysis is alike with the value of 2270 kN provided by the kinematic limit analysis tool. The dome's stability is guaranteed in the absence of iron rings, yet with a very low safety factor (1.06). The good agreement between limit and FE non-linear analysis is also extended to the expected failure mechanisms, as Figure 10 shows that the location of the rotational hinge is coincident for both strategies. It is also important to remark that the observed damage with the FE model corroborates the observations

This paper can be found at: http://dx.doi.org/10.1080/15583058.2021.1992539

reported by Vanvitelli (Como 2013; Le Seur, Jacquier, and Boscovich 1742). In specific, the well-marked and inclined cracking developed in the wall that connects the drum and the buttresses.

6.2. Configuration C2: horizontal thrust of the dome

C2 configuration represents the condition of the dome for which the original iron rings designed by Della Porta were still present. Therefore, the main difference with the previous C1 configuration is the effect of tension iron rings, which provide an increment of stiffness to the system. The computation of the radial stiffness term for both the iron rings, designated as *n* and *u*, was described in Section 4.3 and the values found inserted within the Finite Element (FE) model. For the limit analysis tool, the confinement forces are computed by multiplying the radial stiffness of the iron rings (K_T) computed in section 4.3, by the radial displacement Δr considering the circumferential strain at the yield point. Thus, the confinement forces for the iron rings u and n are equal to 122 kN and are associated with axial stress and elastic modulus equal to 150 MPa and 200 GPa. This stress value corresponds to the assumed iron uniaxial strength, which seems an appropriate initial assumption when assessing ancient iron (Bacigalupo, Brencich, and Gambarotta 2013). Note, however, that the user could adopt any other value of strength, for instance, to represent a current standardized steel class (or other material).

Figure 11 shows the system's horizontal thrust (HT) evolution with the vertical displacement at the dome's crown. Cracking patterns (tension, d_t) have been also plotted for four points, each one associated with a lantern load multiplier λ_{WL}. The FE results are plotted until the load multiplier $\lambda_{\mathrm{WL}} = 1.02$ is reached. The simulation was stopped for such load level, as it represents the yielding of the iron ring positioned in *u*.

This paper can be found at: http://dx.doi.org/10.1080/15583058.2021.1992539

For a $\lambda_{WL} = 1.02$, the cracking is almost absent as reported in Figure 11. It is important to address that the FE analysis could be further developed for increasing values of the load multiplier λ_{WL}, as both the non-linear behaviour of the iron rings and masonry could be further explored. However, such an investigation is out of the scope of the present work to ensure the representativity of the comparison between the FE model and the limit analysis tool. The limit analysis tool simulates the confinement effects of the iron rings through a-priori defined and fixed force values according to the formulation reported in section 4.3, hence neglecting the stiffness degradation of the iron rings. In this context, the horizontal thrust of the FE model (2154 kN) is in good agreement with the one delivered by the kinematic limit analysis (2033 kN) tool, with a difference ranging 6%. The dome faces a lower horizontal thrust when compared with the non-strengthened configuration, which proves the importance of the iron rings as reported in Della Porta's design (Como 2013).

Some cracking in the rib near the crown occurs for a $\lambda_{WL} = 1.0$. Still, significantly lower cracking levels are experienced by the dome if compared with that given for the non-strengthened configuration (see Figure 11 and Figure 12). The safety factor found with limit analysis is automatically provided by the tool and is around 1.33, which clearly demonstrates how the two iron rings allow a 33% extra capacity for the dome when compared to the non-strengthened case.

Such a result validated the results reported in Figure 12, in which the position of the red hinge detected by the limit analysis tool does not reveal an incipient collapse mechanism according to the FE crack patterns.

Furthermore, the dome's thrust ratio was decreased by 11% (from 0.199 to 0.178) allowing the increase of the static efficiency of the system. Note that such

efficiency is evaluated as the ratio between the dome's weight and the resisting horizontal thrust.

At last, it is highlighted that the predicted failure mechanisms by both the kinematic limit analysis and FE analysis are similar, as the formation of a rotational hinge occurs at the same location, specifically on the position where the iron ring that first yields in the FE model (highlighted in a thicker line in Figure 11). A closer observation on the evolution of the stress levels in both iron rings allows concluding that a balanced behaviour is found, despite the different positioning in height. For a $\lambda_{\mathrm{WL}} = 1$, Figure 13 shows that the ring *u* has yielded, and the ring *n* has just near 5% of extra capacity, which clearly advocates the key role that these elements have in lessening the dome's horizontal thrust. Even for $\lambda_{\mathrm{WL}} = 0$, the elastic user percentage (EUP) is around 60%. The EUP is computed as the ratio between the axial stress of the iron ring and its axial strength and, therefore, represents the percentage of the iron ring capacity that is being explored.

6.3. Configuration C3: horizontal thrust of the dome

C3 is the last configuration being analysed and represents the current state of the Vatican dome. Six iron rings were introduced in the 18$^{\mathrm{th}}$ century (cross-section of $56 \times 93\ mm^2$, see Table 2) according to recommendations given by Poleni and Vanvitelli. The contribution of the iron rings in the FE model was modelled by introducing six beam elements embedded in the masonry linked with four springs FEs, as addressed in section 4.

Figure 14 describes the horizontal thrust for C3 structural system as a function of the dome's vertical displacement. The corresponding FE curves for configurations C1 and C2 are also plotted (with grey colour) for comparison purposes. The favourable

confinement effect of the retrofitting system is rather evident. A decreased of the system's horizontal thrust (HT) given as 21% and 18% can be reported with respect to the results from C1 and C2 configurations, respectively. Figure 15 shows that the FE model does not show relevant cracking in the masonry, which proves the effectiveness of the current strengthening system. The iron ring located in the position Z is the one that is subjected to a higher stress level, as depicted in Figure 16, but still has 15% of extra capacity for a lantern weight multiplier of $\lambda_{\mathrm{WL}} = 1$. In converse to the C2 configuration, it seems there is a clear unbalance on the effectiveness of the iron rings, caused by a non-optimal position or by a non-optimal cross-section design. It matters addressing that the latter conclusions are valid for the considered loading cases.

To what concerns the results from the limit analysis, a direct comparison with the FE curve may mislead the reader to conclude on the validity of the limit analysis tool, as the difference in terms of the system's horizontal thrust is significant (around 34% for $\lambda_{\mathrm{WL}} = 1$). A detailed analysis of Figure 16 shows that the comparison lacks representatively. This is so because the confinement forces arising from the iron rings are, within the limit analysis, equal to 305 kN. This value is associated with the iron strength (assumed to be 150 MPa), meaning that an EUP=100% was considered for the limit analysis. The capacity of the rings is being totally explored hence able to decrease the horizontal thrust of the system, which explains why the latter value is below the one provided by the FE model ($\lambda_{\mathrm{WL}} = 1$). In such a context, and for the sake of the limit analysis tool validation, the EUP values found in Figure 16 for the FE analysis ($\lambda_{\mathrm{WL}} = 1$) have been directly defined as input for the limit analysis tool. The updated value for the system's horizontal thrust is obtained within 1 second (real-time) and is now equal to $HT = 1625$ kN, which represents a 11% difference with the value from the FE analysis ($HT = 1820$ kN).

This paper can be found at: http://dx.doi.org/10.1080/15583058.2021.1992539

6.4. An Overview of the Static Efficiency of St. Peter's dome

In 1540, Michelangelo Buonarroti, amazed by the Santa Maria del Fiore's dome proportions, confided: "I'm going to Rome to make your sister, bigger than you, but not more beautiful". St. Peter's dome was indeed built by the drive, knowledge, and passion of Buonarroti and Della Porta. After more than five centuries, there is still an open debate about the most beautiful ancient dome from the Roman Empire. A more objective discussion concerns the static efficiency of such ancient domes. As reported in Como (Como 2013), the domes' efficiency is indirectly proportional to the thrust ratio χ, i.e. the ratio between the horizontal thrust and the total weight of the dome.

Como (Como 2013) computed the thrust ratio for both Santa Maria del Fiore (Florence) and Pantheon (Rome) domes, which are equal to 0.11 and 0.08, respectively (for a unitary lantern load multiplier). The static efficiency of San Peter's dome is characterized by a thrust ratio of 0.185. This value is clearly higher, hence indicating a lower efficiency. It is noteworthy to address that the static efficiency is inversely proportional to the thrust ratio value. Furthermore, one can highlight the fact that the latter value is conditioned by the significant lantern weight of St. Peter's dome. In converse, Pantheon does not present a lantern in his architectural layout and Santa Maria del Fiore's has a larger lantern, yet its total weight is just half of St. Peter's dome.

Figure 17 presents the relationship between the lantern weight multiplier λ_{WL} and the thrust ratio for St. Peter's dome, Brunelleschi's dome, and the Pantheon. Results show that St. Peter's dome has the lowest static efficiency, even for the most favourable scenario characterized by a negligible lantern weight, i.e. $\lambda_{\mathrm{WL}} = 0$. Figure 18 allows concluding that a linear function can, for the range of values analysed, describe the variation of the thrust ratio with λ_{WL}. This can be explained since the total weight of the lantern represents a small percentage of the total weight of the dome.

This paper can be found at: http://dx.doi.org/10.1080/15583058.2021.1992539

Another parametric study was herein conducted to give an insight into the dome's static efficiency for different values of the dome's height. To this aim, the parameter β was defined to update the geometry and it can be described as a scaling parameter that affects only the radius of the extrados shell of St. Peter's dome. Other geometrical dimensions, as the thickness of the shells, thickness of the dome, dimension of the ribs, etc., were kept fixed.

Figure 18a shows the computed relationship between β and the dome's thrust ratio χ, which is non-linear and well approximated by a second-order polynomial. The results demonstrate that the dome's thrust ratio is decreased by increasing the height of the dome (inherent consequence due to the increase of the extrados radius). A direct comparison was also established between the static efficiency of the current geometrical configuration of the dome and the one obtained by a parameter $\beta = 1.4$ (maximum β value admitted). Figure 18b proves the preceding conclusion, in which the thrust ratio decreases from 0.199 to 0.130. A curious remark is that, even for a β=1.4 value, the dome assumes a thrust coefficient equal to 0.13 that still resorts to be higher than the Brunelleschi dome and the Pantheon. At last, this also highlights that such analysis is easily performed using the developed limit analysis tool because the dome's geometry was initially parametrized.

7. Final Remarks

A kinematic limit analysis procedure based on the works of Como (Como 2019; 2013) was implemented in an easy to use tool. The tool provides an automatic procedure for the pre- to the post-processing stage. For the modelling stage, in which the geometry can be parametrized, the commercial software Rhino 3D is recommended (still other pre-processor can be used). For the processing stage, the visual programming tool

Grasshopper was used, as it is quite convenient for integrated and real-time simulations (Block, Ciblac, and Ochsendorf 2006; Rippmann, Lachauer, and Block 2012). The developed Limit Analysis tool aims to support the structural assessment of load carrying capacity of domes. Its mathematical simplicity goes in hand with the ease of use. The resisting horizontal thrust of domes can be computed in a fast and automatic manner and requiring few input parameters.

The worldwide known St. Peter's dome was selected as a case study. It gathers invaluable cultural, historical, and architectural values, but limited studies exist aiming at the comprehension of the structural behaviour within a three-dimensional analysis. It is important to remark that a discussion on the improvement offered by the structural retrofitting of 1743 using six iron rings is valuable and was performed. A FE numerical model based on a macro-modelling approach was adopted for comparison purposes. The CDP model, available in the software ABAQUS (Abaqus 2014), was used and the required material inputs were retrieved from normative recommendations and calibrated to reproduce the reported damage state of the dome after the earthquake events of 1703 and 1730 (Como 2019; 2013). The analyses were conducted on a 1/16 representative slice of the dome. Results include a comparison between the horizontal dome thrust and failure mechanism for both non-strengthened and strengthened configurations. A good agreement was reported, as the results from the limit analysis are slightly lower (related with the no-tension assumption of Heymann theory) when compared with those from the FE model, but still below 4% of difference only. In this regard, it is paramount to acknowledge that a rational approach was developed to compute and simulate the confinement effect of hoop rings in the FE model. Such effect is typically not included in the literature (Bacigalupo, Brencich, and Gambarotta 2013) and was herein suggeste

to be modelled through spring elements whose axial stiffness is dependent on geometrical parameters (ring members and dome) and material properties (ring members). On the other hand, it is also important to address that St. Peter's dome features enables the use of a representative reduced model, i.e. a representative slice of the dome. Note, however, that such modelling assumption is also valid for other domes if the latter symmetry is respected (most of the cases). In a near collapse limit state, meridional cracks tend to appear and cut the dome within slices. This leads to weak transfer of hoop stresses, only possible if strengthening elements are present. Such failure mode is recurrent on domes (Foraboschi 2014; Ventura, et al. 2014) and well-established in other studies (Bartoli, Betti, and Borri 2015; Bacigalupo, Brencich, and Gambarotta 2013) guaranteeing, therefore, the representativity and generalization of the limit analysis strategy.

The importance of the tool is especially noted when the knowledge of a proper reference value for the dome's horizontal thrust is useful; even in the case in which results from a more advanced strategy, as the CDP model addressed in this study, need further validation. The quasi-brittle nature of masonry offers a challenge when characterizing its non-linear mechanical behaviour, as mode-I fracture energies significantly affect the capacity often requiring full-scale testing (Fanning, and Boothby 2001). Although a complex and detailed analysis may provide valuable information – as the load capacity, the expected cracking pattern, and the ductility level of the structure – , it may be addressed that the input uncertainty is high in most of the cases and the computational effort is significant. The proposed limit analysis tool requires only 1-2 seconds per analysis (real-time results).

The proposed tool is made available online as supplementary material aiming to cope with the uncertainty associated when analysing masonry domes, but also to give a

reasonable estimation on the static horizontal thrust of domes for a structural safety evaluation study. Future research may include further development of the strategy to make it eligible for the study of other strengthening techniques, such as the use of Textile Reinforced Matrix (TRM) of Fiber Reinforced Polymers (FRP) reinforcement and considering both shape and material optimization.

Competing interest: The authors declare no competing interest

References:

Abaqus, Version. 2014. "6.14 Documentation." *Dassault Systemes Simulia Corporation* 651 (6.2).

Anselmi, C., F. Galizia, and E. Saetta. 2020. "3D Limit Analysis of Masonry Pavilion Domes on Octagonal Drum Subjected to Vertical Loads." *Frattura Ed Integrita Strutturale* 14 (51): 486–503. https://doi.org/10.3221/IGF-ESIS.51.37.

Bacigalupo, A., A. Brencich, and L. Gambarotta. 2013. "A Simplified Assessment of the Dome and Drum of the Basilica of S. Maria Assunta in Carignano in Genoa." *Engineering Structures* 56 (November): 749–65. https://doi.org/10.1016/J.ENGSTRUCT.2013.05.006.

Baldrati, Barbara. 2009. "LA CUPOLA DELLA BASILICA DI SAN PIETRO IN VATICANO. IL CANTIERE E IL SISTEMA COSTRUTTIVO."

Bartoli, Gianni, Michele Betti, and Claudio Borri. 2015. "Numerical Modeling of the Structural Behavior of Brunelleschi's Dome of Santa Maria Del Fiore." *Http://Dx.Doi.Org/10.1080/15583058.2013.797038* 9 (4): 408–29. https://doi.org/10.1080/15583058.2013.797038.

Belluzzi, Odone. 1946. *Scienza Delle Costruzioni...* Vol. 1. N. Zanichelli.

Block, Philippe, Thierry Ciblac, and John Ochsendorf. 2006. "Real-Time Limit Analysis of Vaulted Masonry Buildings." *Computers & Structures* 84 (29–30): 1841–52. https://doi.org/10.1016/J.COMPSTRUC.2006.08.002.

Brumana, Raffaella, Stefano Della Torre, Daniela Oreni, Lorenzo Cantini, Mattia Previtali, Luigi Barazzetti, and Fabrizio Banfi. 2018. "SCAN to HBIM-Post Earthquake Preservation: Informative Model as Sentinel at the Crossroads of Present, Past, and Future." In *Lecture Notes in Computer Science (Including Subseries Lecture Notes in Artificial Intelligence and Lecture Notes in Bioinformatics)*, 11196 LNCS:39–51. Springer Verlag. https://doi.org/10.1007/978-3-030-01762-0_4.

Bussi, Laura, Marta Carusi, and Paolo Rocchi. 2009. *Nuove Ricerche Sulla Gran Cupola Del Tempio Vaticano*. Arti Grafiche Editoriali.

Cascardi, A., F. Micelli, M.A. Aiello, and M. Funari. 2020. "Structural Analysis of a

Masonry Church with Variable Cross-Section Dome." In *Brick and Block Masonry - From Historical to Sustainable Masonry*, 220–26. CRC Press. https://doi.org/10.1201/9781003098508-28.

Cavalagli, Nicola, and Vittorio Gusella. 2014. "Dome of the Basilica of Santa Maria Degli Angeli in Assisi: Static and Dynamic Assessment." *Http://Dx.Doi.Org/10.1080/15583058.2014.951799* 9 (2): 157–75. https://doi.org/10.1080/15583058.2014.951799.

Cennamo, Claudia, and Concetta Cusano. 2020. "THE 'BAROQUE SKYLINE' IN NAPLES. STRUCTURAL STUDIES ON 16TH AND 17TH CENTURY DOMES IN TERMS OF FORM AND STABILITY." *Architecture and Engineering* 5 (2): 08–16. https://doi.org/10.23968/2500-0055-2020-5-2-08-16.

Chiozzi, Andrea, Gabriele Milani, Nicola Grillanda, and Antonio Tralli. 2017. "A Fast and General Upper-Bound Limit Analysis Approach for out-of-Plane Loaded Masonry Walls." *Meccanica 2017 53:7* 53 (7): 1875–98. https://doi.org/10.1007/S11012-017-0637-X.

Como, Mario. 2013. *Statics of Historic Masonry Constructions*. Vol. 1. Springer.

———. 2019. "Thrust Evaluations of Masonry Domes. An Application to the St. Peter's Dome." *International Journal of Masonry Research and Innovation* 4 (1–2): 32–49. https://doi.org/10.1504/IJMRI.2019.096823.

Croce, M. Di, Felice C. Ponzo, and Mauro Dolce. 2010. "Design of the Seismic Upgrading of the Tambour of the S. Nicolò's Church in Catania with the DIS-CAM System." *Advanced Materials Research* 133–134: 947–52. https://doi.org/10.4028/WWW.SCIENTIFIC.NET/AMR.133-134.947.

Cundari, G. A., G. Milani, and G. Failla. 2017. "Seismic Vulnerability Evaluation of Historical Masonry Churches: Proposal for a General and Comprehensive Numerical Approach to Cross-Check Results." *Engineering Failure Analysis* 82 (December): 208–28. https://doi.org/10.1016/j.engfailanal.2017.08.013.

Diz-Mellado, Eduardo, Emilio J. Mascort-Albea, Rocío Romero-Hernández, Carmen Galán-Marín, Carlos Rivera-Gómez, Jonathan Ruiz-Jaramillo, and Antonio Jaramillo-Morilla. 2021. "Non-Destructive Testing and Finite Element Method Integrated Procedure for Heritage Diagnosis: The Seville Cathedral Case Study." *Journal of Building Engineering* 37 (May): 102134. https://doi.org/10.1016/J.JOBE.2020.102134.

e dei Trasporti, Ministero delle Infrastrutture. 2019. "Circolare 21 Gennaio 2019 n. 7 Istruzioni per l'applicazione Dell'Aggiornamento Delle Nuove Norme Tecniche per Le Costruzioni Di Cui Al Decreto Ministeriale 17 Gennaio 2018." GU.

Fabbrocino, Francesco, Marco Francesco Funari, Fabrizio Greco, Paolo Lonetti, and Raimondo Luciano. 2020. "Numerical Modeling Based on Moving Mesh Method to Simulate Fast Crack Propagation." *Frattura Ed Integrita Strutturale* 14 (51): 410–22. https://doi.org/10.3221/IGF-ESIS.51.30.

Fanning, Paul J, and Thomas E Boothby. 2001. "Three-Dimensional Modelling and Full-Scale Testing of Stone Arch Bridges." *Computers & Structures* 79 (29): 2645–62. https://doi.org/https://doi.org/10.1016/S0045-7949(01)00109-2.

Feizolahbeigi, Arezu, Paulo B. Lourenço, Mahmoud Golabchi, Javier Ortega, and Mojtaba Rezazadeh. 2021. "Discussion of the Role of Geometry, Proportion and

Construction Techniques in the Seismic Behavior of 16th to 18th Century Bulbous Discontinuous Double Shell Domes in Central Iran." *Journal of Building Engineering* 33 (January): 101575. https://doi.org/10.1016/J.JOBE.2020.101575.

Fontana, Carlo. 1694. "1694. Il Tempio Vaticano e Sua Origine." *Con Gli Edifitii Cospicui Antichi, e Moderni Fatti Dentro e Fuori Di Esso. Rome: Gio. Francesco Buagni*.

Foraboschi, Paolo. 2014. "Resisting System and Failure Modes of Masonry Domes." *Engineering Failure Analysis* 44 (September): 315–37. https://doi.org/10.1016/J.ENGFAILANAL.2014.05.005.

Fortunato, G., M.F. Funari, and P. Lonetti. 2017. "Survey and Seismic Vulnerability Assessment of the Baptistery of San Giovanni in Tumba (Italy)." *Journal of Cultural Heritage*. https://doi.org/10.1016/j.culher.2017.01.010.

Funari, M.F., S. Spadea, M. Ciantia, P. Lonetti, and F. Greco. 2020. "Visual Programming for the Structural Assessment of Historic Masonry Structures." In *REHABEND*.

Funari, Marco Francesco, Anjali Mehrotra, and Paulo B. Lourenço. 2021. "A Tool for the Rapid Seismic Assessment of Historic Masonry Structures Based on Limit Analysis Optimisation and Rocking Dynamics." *Applied Sciences (Switzerland)* 11 (3): 1–22. https://doi.org/10.3390/app11030942.

Funari, Marco Francesco, Saverio Spadea, Paolo Lonetti, Francesco Fabbrocino, and Raimondo Luciano. 2020. "Visual Programming for Structural Assessment of Out-of-Plane Mechanisms in Historic Masonry Structures." *Journal of Building Engineering* 31 (September). https://doi.org/10.1016/j.jobe.2020.101425.

Gaetani, Angelo, Giorgio Monti, Paulo B. Lourenço, and Giancarlo Marcari. 2016. "Design and Analysis of Cross Vaults Along History." *International Journal of Architectural Heritage* 10 (7): 841–56. https://doi.org/10.1080/15583058.2015.1132020.

Ginovart, J. Lluís i, A. Costa, and G. Fortuny. 2013. "Assessment And Restoration Of A Masonry DomeIn The Cathedral Of Tortosa Enclosure." *WIT Transactions on The Built Environment* 131 (June): 391–401. https://doi.org/10.2495/STR130331.

"Grasshopper - Algorithmic Modeling for Rhino." 2020. 2020. https://www.grasshopper3d.com/.

Hejazi, Mehrdad, and Masih Pourabedin. 2021. "Performance of Persian Brick Masonry Discontinuous Double-Shell Domes against Earthquakes." *Engineering Failure Analysis* 119 (January): 104994. https://doi.org/10.1016/J.ENGFAILANAL.2020.104994.

Heyman, Jacques. 1966. "The Stone Skeleton." *International Journal of Solids and Structures* 2 (2): 249–79. https://doi.org/10.1016/0020-7683(66)90018-7.

———. 1969. "The Safety of Masonry Arches." *International Journal of Mechanical Sciences* 11 (4): 363–85. https://doi.org/10.1016/0020-7403(69)90070-8.

HUERTA FERNANDEZ, S. 1990. "Structural Design of Arches, Vaults and Domes in Spain: 1500-1800." *Doctoral Disseitation in Progress under the Direction of Professor R. Aroca Hernández-Ros*.

Jasieńko, Jerzy, Krzysztof Raszczuk, Kajetan Kleszcz, and Piotr Frąckiewicz. 2021.

"Numerical Analysis of Historical Masonry Domes: A Study of St. Peter's Basilica Dome." *Structures* 31 (June): 80–86. https://doi.org/10.1016/J.ISTRUC.2021.01.082.

Lagarias, Jeffrey C, James A Reeds, Margaret H Wright, and Paul E Wright. 1998. "Convergence Properties of the Nelder--Mead Simplex Method in Low Dimensions." *SIAM Journal on Optimization* 9 (1): 112–47.

Lemos, José V. 2007. "Discrete Element Modeling of Masonry Structures." *International Journal of Architectural Heritage* 1 (2): 190–213. https://doi.org/10.1080/15583050601176868.

López López, David, Pere Roca, Andrew Liew, Tom Van Mele, and Philippe Block. 2019. "Tile Vaults as Integrated Formwork for Reinforced Concrete: Construction, Experimental Testing and a Method for the Design and Analysis of Two-Dimensional Structures." *Engineering Structures* 188 (June): 233–48. https://doi.org/10.1016/J.ENGSTRUCT.2019.03.034.

Lourenço, P.B. 1997. "Computational Strategies for Masonry Structures." 1997. https://www.elibrary.ru/item.asp?id=6874848.

Lourenço, Paulo B., and Luís C. Silva. 2020. "Computational Applications in Masonry Structures: From the Meso-Scale to the Super-Large/Super-Complex." *International Journal for Multiscale Computational Engineering* 18 (1): 1–30. https://doi.org/10.1615/IntJMultCompEng.2020030889.

Lubliner, J., J. Oliver, S. Oller, and E. Oñate. 1989. "A Plastic-Damage Model for Concrete." *International Journal of Solids and Structures* 25 (3): 299–326. https://doi.org/10.1016/0020-7683(89)90050-4.

Macchi, G. 2001. "Diagnosis of the Facade of St. Peter's Basilica in Rome." *Historical Constructions. Universidade Do Minho: Guimarães*, 309–17.

Maria D'altri, Antonio, Vasilis Sarhosis, Gabriele Milani, Jan Rots, Serena Cattari, Sergio Lagomarsino, Elio Sacco, Antonio Tralli, Giovanni Castellazzi, and Stefano De Miranda. 2020. "Modeling Strategies for the Computational Analysis of Unreinforced Masonry Structures: Review and Classification" 27: 1153–85. https://doi.org/10.1007/s11831-019-09351-x.

Mehrotra, A., A. Arede, and M. J. DeJong. 2015. "Discrete Element Modeling of a Post-Tensioned Masonry Arch." *Civil-Comp Proceedings*. https://doi.org/10.4203/CCP.108.49.

Milani, G. 2015. "Upper Bound Sequential Linear Programming Mesh Adaptation Scheme for Collapse Analysis of Masonry Vaults." *Advances in Engineering Software* 79 (January): 91–110. https://doi.org/10.1016/J.ADVENGSOFT.2014.09.004.

Milani, G., and A. Cecchi. 2013. "Compatible Model for Herringbone Bond Masonry: Linear Elastic Homogenization, Failure Surfaces and Structural Implementation." *International Journal of Solids and Structures* 50 (20–21): 3274–96. https://doi.org/10.1016/J.IJSOLSTR.2013.05.032.

Milani, G., P. B. Lourenço, and A. Tralli. 2006. "Homogenised Limit Analysis of Masonry Walls, Part I: Failure Surfaces." *Computers & Structures* 84 (3–4): 166–80. https://doi.org/10.1016/J.COMPSTRUC.2005.09.005.

Milani, Gabriele, Michele Simoni, and Antonio Tralli. 2014. "Advanced Numerical

Models for the Analysis of Masonry Cross Vaults: A Case-Study in Italy." *Engineering Structures* 76 (1): 339–58. https://doi.org/10.1016/j.engstruct.2014.07.018.

Milani, Gabriele, Marco Valente, Mario Fagone, Tommaso Rotunno, and Claudio Alessandri. 2019. "Advanced Non-Linear Numerical Modeling of Masonry Groin Vaults of Major Historical Importance: St John Hospital Case Study in Jerusalem." *Engineering Structures* 194 (September): 458–76. https://doi.org/10.1016/J.ENGSTRUCT.2019.05.021.

Mordà, Nicola, and Alfonso Mancini. 2018. "Norme Tecniche per Le Costruzioni (NTC 2018) D. Min. Infrastrutture e Trasporti 17 Gennaio 2018." Legislazione tecnica.

O'Dwyer, Dermot. 1999. "Funicular Analysis of Masonry Vaults." *Computers & Structures* 73 (1–5): 187–97. https://doi.org/10.1016/S0045-7949(98)00279-X.

Pepe, Marco, Marco Pingaro, and Patrizia Trovalusci. 2021. "Limit Analysis Approach for the In-Plane Collapse of Masonry Arches." *Https://Doi.Org/10.1680/Jencm.20.00013* 174 (2): 66–81. https://doi.org/10.1680/JENCM.20.00013.

Pepe, Marco, Marialuigia Sangirardi, Emanuele Reccia, Marco Pingaro, Patrizia Trovalusci, and Gianmarco de Felice. 2020. "Discrete and Continuous Approaches for the Failure Analysis of Masonry Structures Subjected to Settlements." *Frontiers in Built Environment* 0 (April): 43. https://doi.org/10.3389/FBUIL.2020.00043.

Poleni, Giovanni. 1982. *Memorie Istoriche Della Gran Cvpola [Cupola] Del Tempio Vaticano, e de'danni Di Essa, e de'ristoramenti Loro, Divise in Libri Cinqve: Repr. Der. Ausg. 1748*. Intemac.

Portioli, F., C. Casapulla, M. Gilbert, and L. Cascini. 2014. "Limit Analysis of 3D Masonry Block Structures with Non-Associative Frictional Joints Using Cone Programming." *Computers and Structures* 143 (September): 108–21. https://doi.org/10.1016/j.compstruc.2014.07.010.

Prieto, A. J., J. M. Macías-Bernal, María-José Chávez, F. J. Alejandre, and A. Silva. 2019. "Impact of Maintenance, Rehabilitation, and Other Interventions on Functionality of Heritage Buildings." *Journal of Performance of Constructed Facilities* 33 (2): 04019011. https://doi.org/10.1061/(ASCE)CF.1943-5509.0001271.

"Rhino - Rhinoceros 3D." 2020. 2020. https://www.rhino3d.com/.

Rippmann, Matthias, Lorenz Lachauer, and Philippe Block. 2012. "Interactive Vault Design." *International Journal of Space Structures* 27 (4): 219–30. https://doi.org/10.1260/0266-3511.27.4.219.

Sanctis, Aldo De, Antonio Lio, Nicola Totaro, and Antonio A Zappani. 2018. "La Basilica Di San Pietro: Rilievi Come Modelli Di Conoscenza (XVII e XVIII Secolo)." *Diségno*, no. 3: 203–12.

Savalle, Nathanaël, Éric Vincens, and Stéphane Hans. 2020. "Experimental and Numerical Studies on Scaled-down Dry-Joint Retaining Walls: Pseudo-Static Approach to Quantify the Resistance of a Dry-Joint Brick Retaining Wall." *Bulletin of Earthquake Engineering* 18 (2): 581–606. https://doi.org/10.1007/s10518-019-00670-9.

Scacco, J., G. Milani, and Paulo B. Lourenço. 2020. “Automatic Mesh Generator for the Non-Linear Homogenized Analysis of Double Curvature Masonry Structures.” *Advances in Engineering Software* 150 (December). https://doi.org/10.1016/J.ADVENGSOFT.2020.102919.

Seur, T Le, F Jacquier, and R G Boscovich. 1742. “Parere Di Tre Matematici Sopra i Danni Che Si Sono Trovati Nella Cupola Di San Pietro.” Roma.

Sharifi, Ali. 2020. “Most Appropriate Time for the Adaptive Reuse of Historic Buildings Using ARP Model.” *Property Management* 38 (1): 109–23. https://doi.org/10.1108/PM-07-2019-0039.

Sharma, S., L. C. Silva, F. Graziotti, G. Magenes, and G. Milani. 2021. “Modelling the Experimental Seismic Out-of-Plane Two-Way Bending Response of Unreinforced Periodic Masonry Panels Using a Non-Linear Discrete Homogenized Strategy.” *Engineering Structures* 242 (September): 112524. https://doi.org/10.1016/J.ENGSTRUCT.2021.112524.

Silva, Luís C., Nuno Mendes, Paulo B. Lourenço, and Jason Ingham. 2018. “Seismic Structural Assessment of the Christchurch Catholic Basilica, New Zealand.” *Structures* 15 (August): 115–30. https://doi.org/10.1016/J.ISTRUC.2018.06.004.

Simon, József, and Katalin Bagi. 2014. “Discrete Element Analysis of the Minimum Thickness of Oval Masonry Domes.” *Http://Dx.Doi.Org/10.1080/15583058.2014.996921* 10 (4): 457–75. https://doi.org/10.1080/15583058.2014.996921.

Sorrentino, Luigi, Laura Liberatore, Luis D. Decanini, and Domenico Liberatore. 2013. “The Performance of Churches in the 2012 Emilia Earthquakes.” *Bulletin of Earthquake Engineering 2013 12:5* 12 (5): 2299–2331. https://doi.org/10.1007/S10518-013-9519-3.

“The Dome of St Peter’s: Structural Aspects of Its Design and Construction, and Inquiries into Its Stability on JSTOR.” 1999. 1999. https://www.jstor.org/stable/29544154?seq=1#metadata_info_tab_contents.

“The Python Language Reference — Python 3.9.5 Documentation.” 2021. 2021. https://docs.python.org/3/reference/.

Turco, C., M.F. Funari, S. Spadea, M. Ciantia, and P.B. Lourenço. 2020. “A Digital Tool Based on Genetic Algorithms and Limit Analysis for the Seismic Assessment of Historic Masonry Buildings.” In *Procedia Structural Integrity*. Vol. 28. https://doi.org/10.1016/j.prostr.2020.10.124.

“Vatican City - UNESCO World Heritage Centre.” 2021. 2021. https://whc.unesco.org/en/list/286/.

Ventura, Giulio, Marco Coppola, Chiara Calderini, and Mario Alberto Chiorino. 2014. “Three-Dimensional Limit Analysis of the Vicoforte Elliptical Dome.” *Http://Dx.Doi.Org/10.1080/15583058.2012.704658* 8 (5): 649–69. https://doi.org/10.1080/15583058.2012.704658.

Willis, C.R., M.C. Griffith, and S.J. Lawrence. 2004. “Horizontal Bending of Unreinforced Clay Brick Masonry.” *Masonry International* 17 (3): 109–21.

This paper can be found at: http://dx.doi.org/10.1080/15583058.2021.1992539

Table 1: Parameters adopted in the simulations for the CDP model.

Material properties	**Values**
Density	1850 $Kg.m^{-3}$
Elastic Modulus	1950 N/mm^2
Poisson ratio	0.2
Tensile strength	0.22425 N/mm^2
Compressive strength	4.485 N/mm^2
Dilation angle	10 degrees
Eccentricity	0.1
f_{b0}/f_{c0}	1.16
K_c	0.667
Viscosity Parameter	0.002

This paper can be found at: http://dx.doi.org/10.1080/15583058.2021.1992539

Table 2 : Geometrical and mechanical properties of the iron rings.

Ring	**radius [m]**	**E_I [N/m^2]**	**t [m]**	**H [m]**	**Area [m^2]**	**K_T [N·m^{-1}]**
u	23.2	200×10^9	0.037	0.056	0.002	7021094
n	24.3	200×10^9	0.037	0.056	0.002	6714572
A	24.3	200×10^9	0.056	0.093	0.005	14545843
B	24.3	200×10^9	0.056	0.093	0.005	16738173.
C	24.3	200×10^9	0.056	0.093	0.005	16738173
D	19.7	200×10^9	0.056	0.093	0.005	20668079
E	5.7	200×10^9	0.056	0.093	0.005	71629968
Z	23.7	200×10^9	0.056	0.093	0.005	17226311

This paper can be found at: http://dx.doi.org/10.1080/15583058.2021.1992539

This paper can be found at: http://dx.doi.org/10.1080/15583058.2021.1992539

Figure 12. Comparison of the failure mechanism for the configuration C2 obtained with the kinematic limit analysis tool and the damage pattern found with the FE non-linear analysis for a $\lambda_{WL} = 1$.

Figure 13. Effectiveness of the iron rings for the configuration C2 given by the elastic usage percentage (EUP, given as the elastic stress/strength).

Figure 14. Obtained results for the configuration C3 in terms of dome's horizontal thrust and damage evolution.

Figure 15. Comparison of the failure mechanism for the configuration C3 obtained with the kinematic limit analysis tool and the damage pattern found with the FE non-linear analysis for a $\lambda_{WL} = 1$.

Figure 16. Effectiveness of the iron rings for the configuration C3 given by the elastic usage percentage (EUP, given as the elastic stress/strength).

Figure 17: Relationship between the lantern load multiplier and the static efficiency for St. Peter's dome, Brunelleschi's dome, and the Pantheon.

Figure 18: (a) Comparison between thrust ratio values for St. Peter's dome, Brunelleschi's dome, and the Pantheon; and (b) thrust ratio for St. Peter's dome for $\beta = 1.0$ (current geometry) and for $\beta = 1.4$ (hypothetical geometry).

(a) (b)

(a) (b)

Figure 1: St. Peter's (a) Basilica and (b) geometrical model of the dome, which was selected as a case study. Figure 1a by Alvesgaspar - Own work, CC BY-SA 4.0, https://commons.wikimedia.org/w/index.php?curid=43509289.

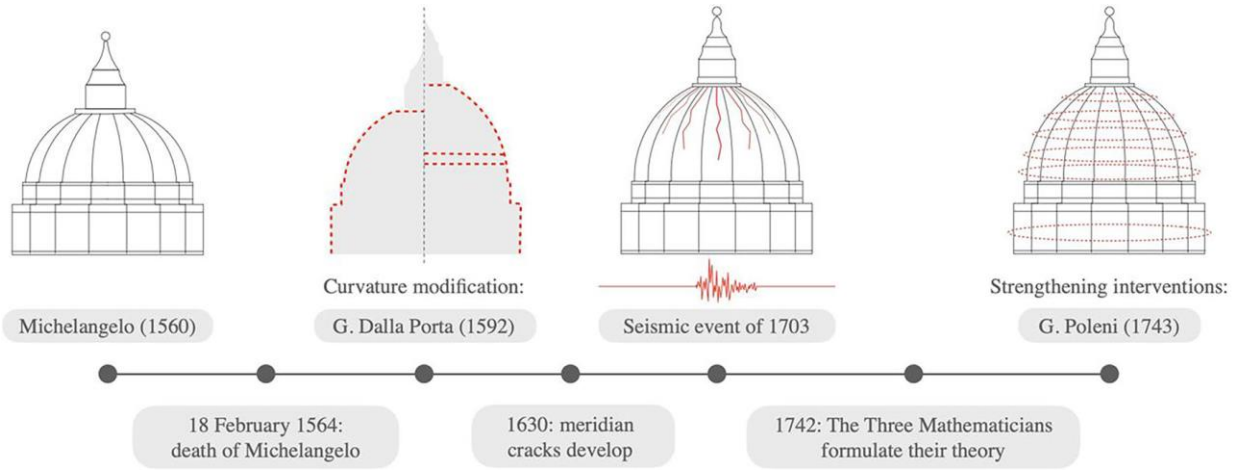

Figure 2: Timeline with the main structural modifications conducted in St. Peter's dome (the iron rings nomenclature added in 1743 follow the original drawings from Poleni).

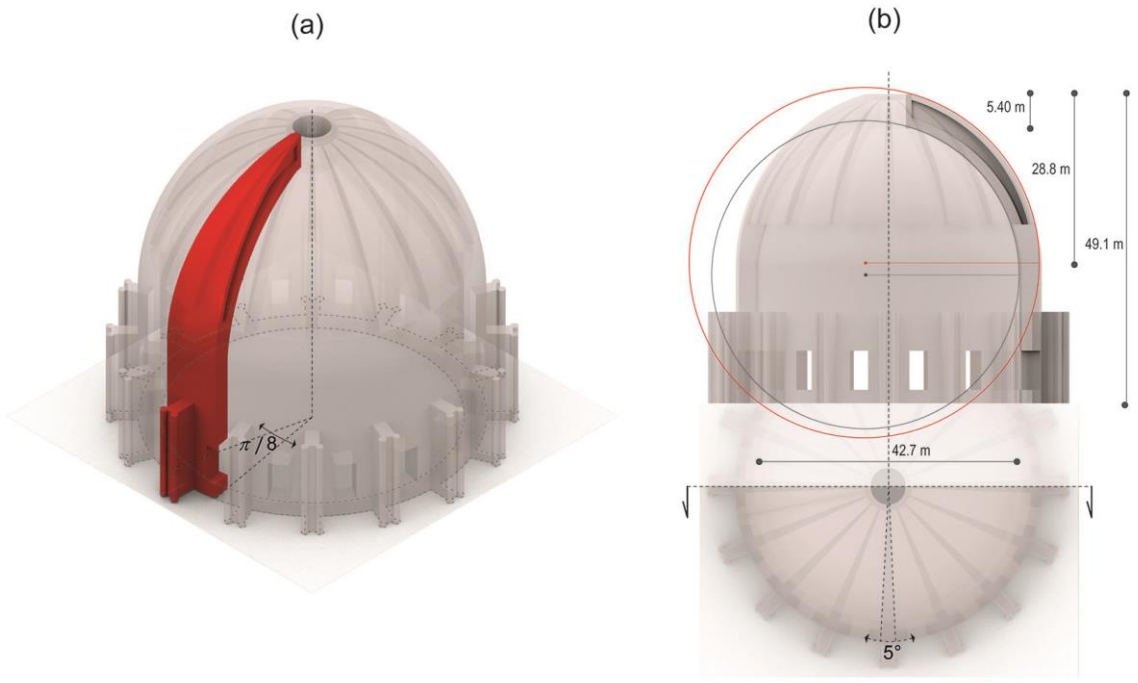

Figure 3: Geometry of St. Peter's dome (a) representation of a 1/16 slice; and (b) parametrization.

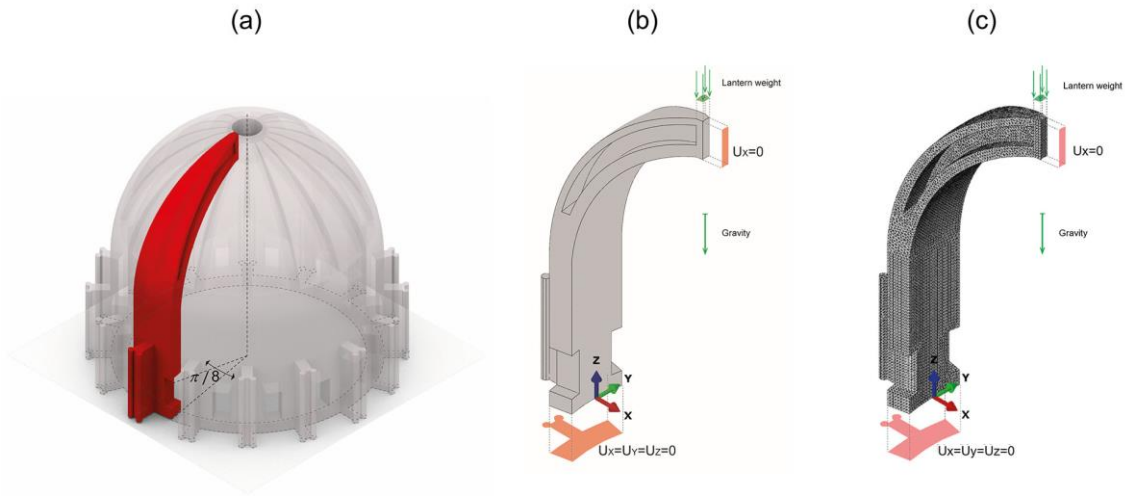

Figure 4: St. Peter's dome: (a) full three-dimensional geometry, (b) three-dimensional geometry of the analysed 1/16 slice with a description of the applied boundary and loading conditions; and (c) FE numerical mesh.

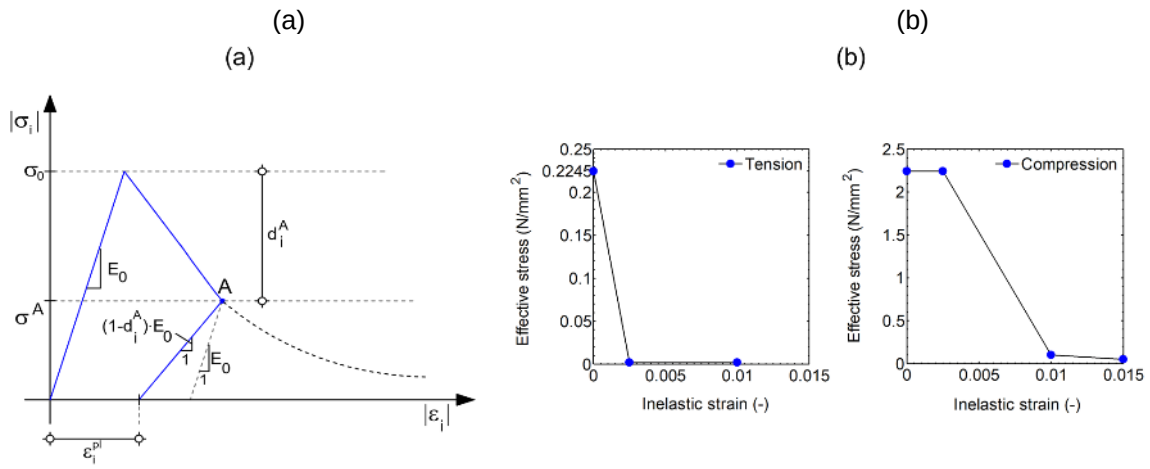

Figure 5: (a) Stress-strain non-linear relationship reproduced by the CDP model. (b) Input for the tension and compression regimes for the CDP model: stress vs inelastic strain.

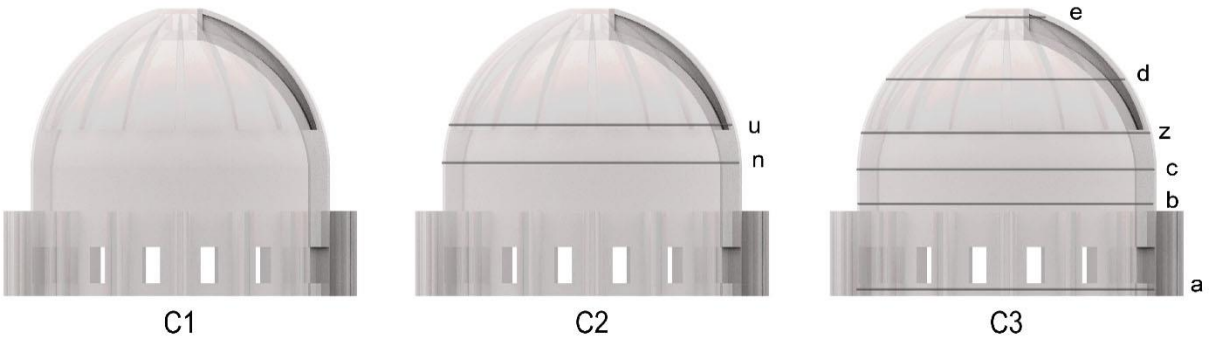

Figure 6: Schematic representation of the three analysed configurations of the dome.

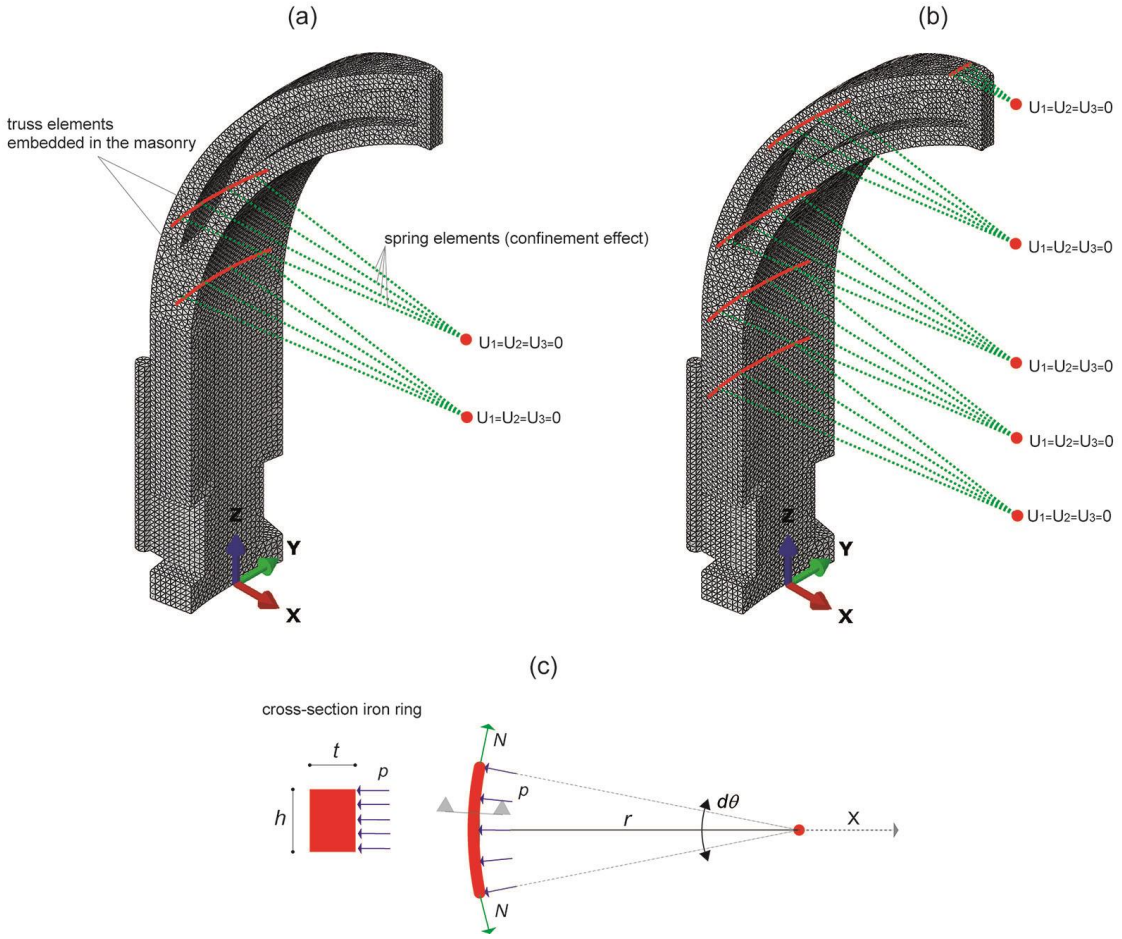

Figure 7: FE-modelling of the iron rings for the configuration (a) C1 and (b) C2. (c) Internal equilibrium on the studied 1/16 slice to compute the confinement effect of the iron rings.

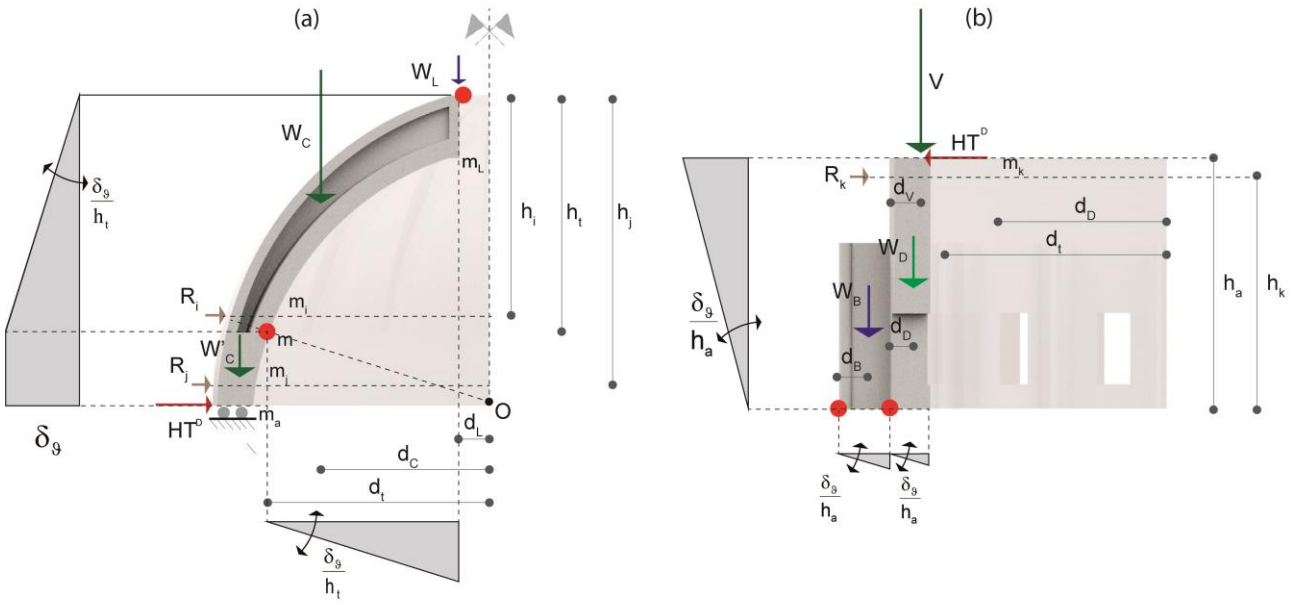

Figure 8: Kinematic description of the failure mechanism for the (a) dome and (b) retaining system (attic-drum-buttress).

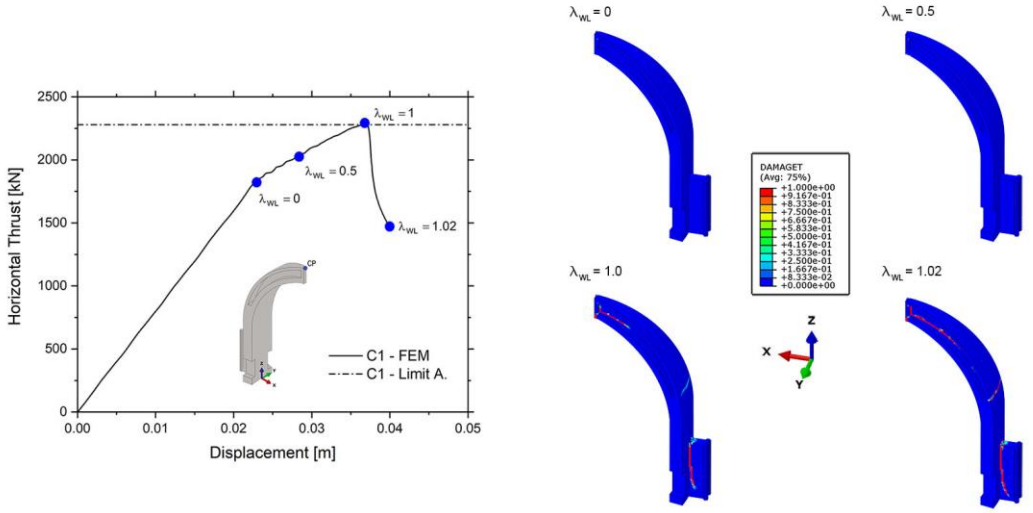

Figure 9: Obtained results for the configuration C1 in terms of dome's horizontal thrust and damage evolution.

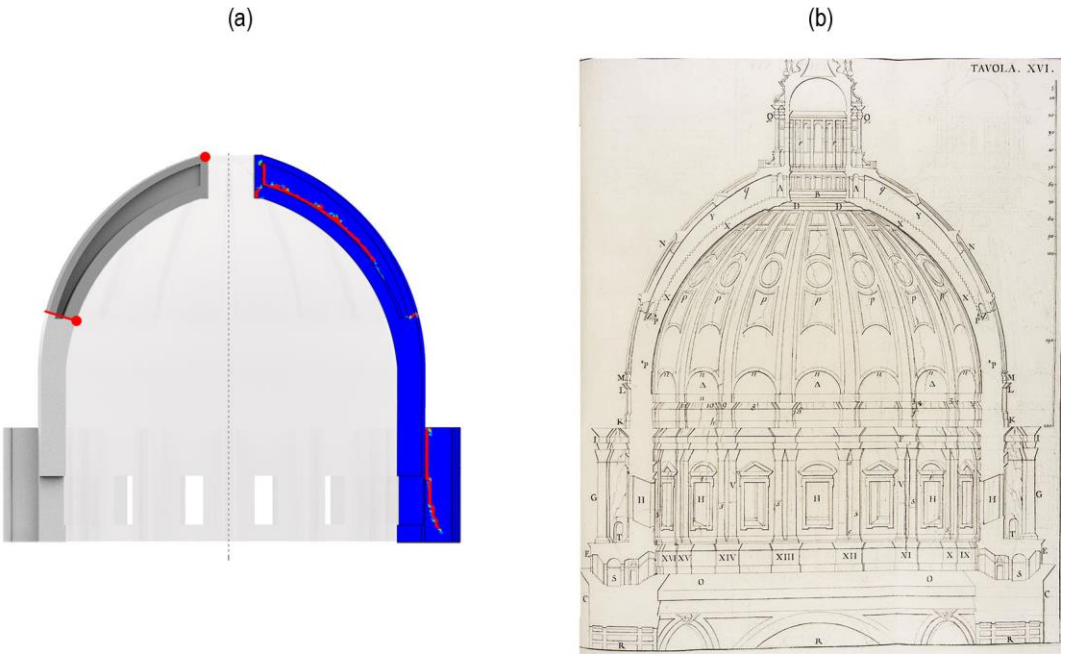

Figure 10: (a) Comparison of the failure mechanism for the configuration C1 obtained with the kinematic limit analysis tool and the FE non-linear analysis, (b) Vanvitelli, damage detected on the buttresses (1743-1748)

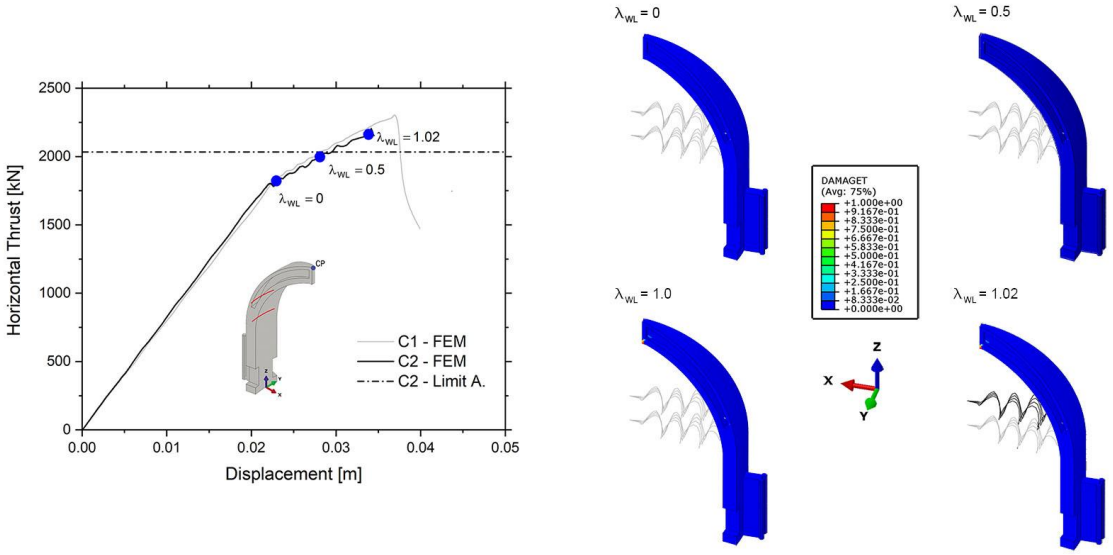

Figure 11: Obtained results for the configuration C2 in terms of dome's horizontal thrust and damage evolution.

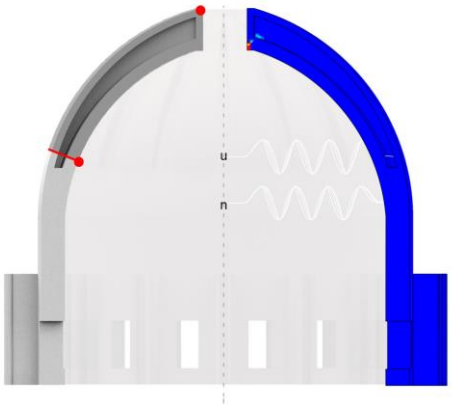

Figure 12: Comparison of the failure mechanism for the configuration C2 obtained with the kinematic limit analysis tool and the damage pattern found with the FE non-linear analysis for a $\lambda_{WL} = 1$.

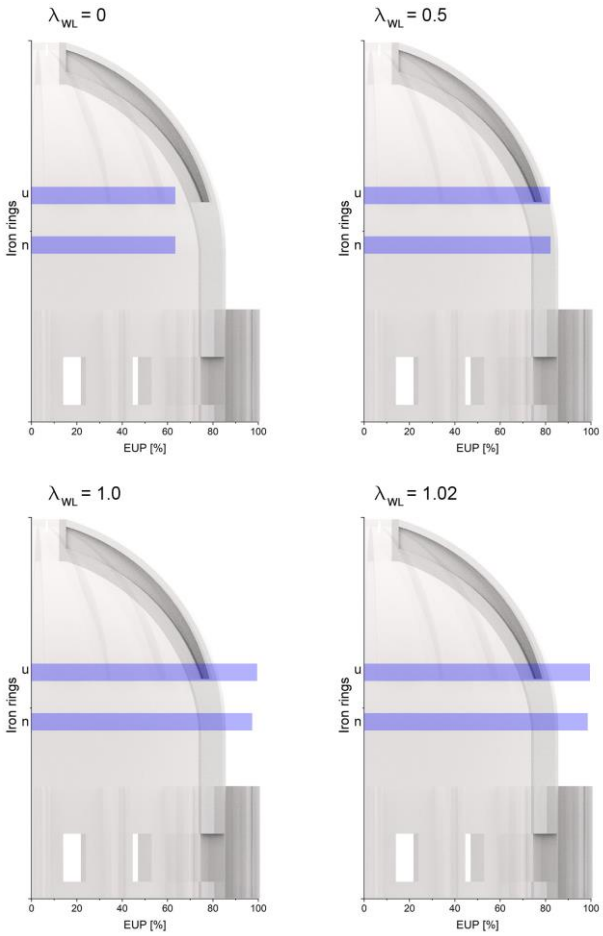

198

199 Figure 13: Effectiveness of the iron rings for the configuration C2 given by the elastic usage percentage (EUP, given
200 as the elastic stress/strength).

201

202

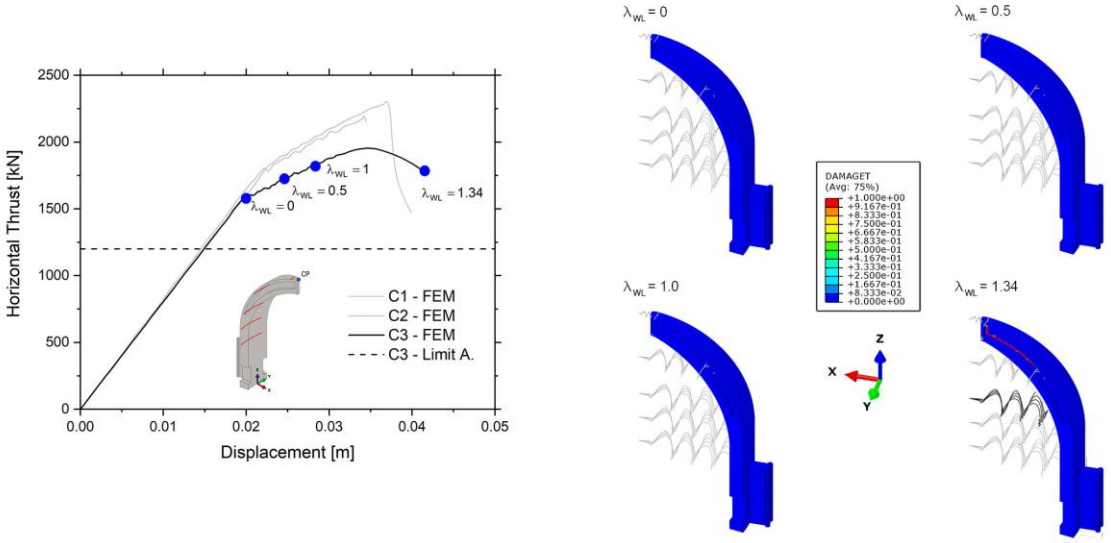

Figure 14: Obtained results for the configuration C3 in terms of dome's horizontal thrust and damage evolution.

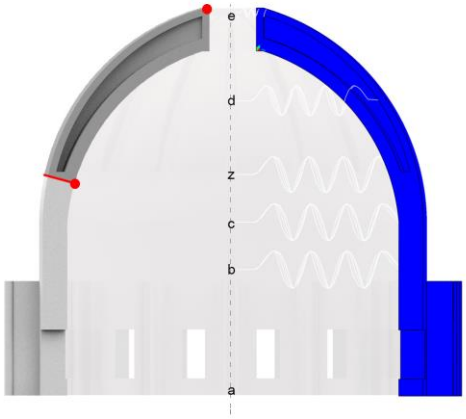

224

225 Figure 15: Comparison of the failure mechanism for the configuration C3 obtained with the kinematic limit analysis
226 tool and the damage pattern found with the FE non-linear analysis for a $\lambda_{\mathrm{WL}} = 1$.

227

228

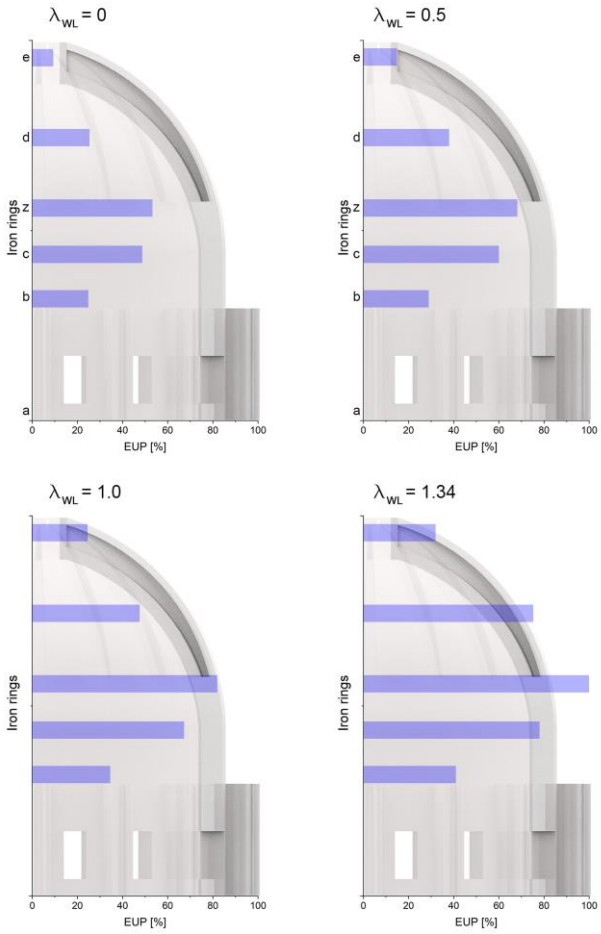

229

230 Figure 16: Effectiveness of the iron rings for the configuration C3 given by the elastic usage percentage (EUP, given
231 as the elastic stress/strength).
232

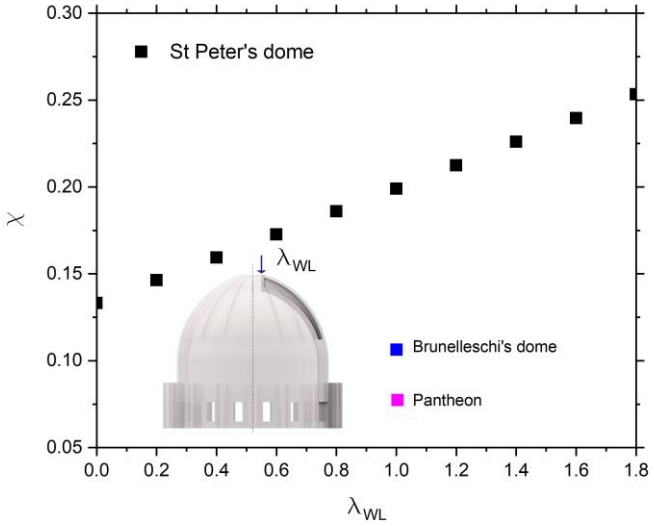

Figure 17: Relationship between the lantern load multiplier and the static efficiency for St. Peter's dome, Brunelleschi's dome, and the Pantheon.

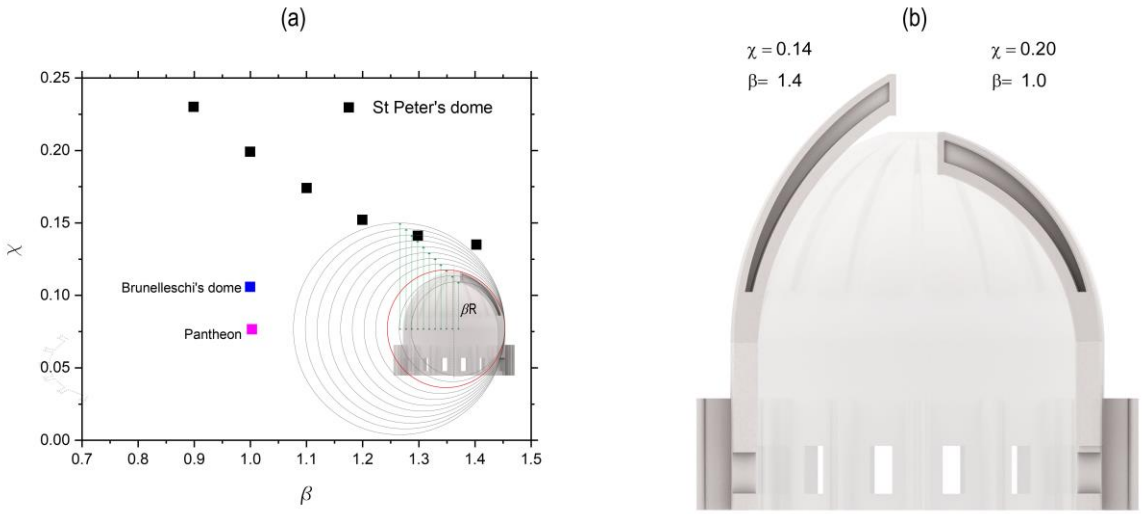

Figure 18: (a) Comparison between thrust ratio values for St. Peter's dome, Brunelleschi's dome, and the Pantheon; and (b) thrust ratio for St. Peter's dome for $\beta = 1.0$ (current geometry) and for $\beta = 1.4$ (hypothetical geometry).